scientific reports

Check for updates

OPEN

Sex-dependent modulation of PCB-mediated toxicity from a proteomic and microbiome perspective

Richa Singhal[1,2], Zayna Qaissi[3], Hao Zheng[4], Yuan Hua[3], Josiah E. Hardesty[5,6], Eric C. Rouchka[2], Michael L. Merchant[4,7], Maiying Kong[4,8,9] & Banrida Wahlang[3,4,5,6,10]✉

Polychlorinated biphenyls (PCBs) have been associated with sex-dependent liver disease outcomes. Current mechanisms only partially explain these sex differences and alternative mechanisms including gut-liver toxicity warrant investigation. This study aims to identify PCB-induced changes in the hepatic proteome and gut microbiome and determine their contributions to sex-specific PCB toxicity. Male and female C57BL/6J mice were exposed to Aroclor1260 (20 mg/kg) and PCB126 (20 µg/kg) via oral gavage. After two weeks, hepatic and intestinal tissues were collected for peptide measurements (LC/MS) and 16S sequencing respectively. Proteomic analysis revealed that biological sex largely drove differences seen in the hepatic proteome and dictated PCB liver responses. PCB-exposed females manifested higher abundance of aryl hydrocarbon receptor (AHR) targets including CD36 vs. PCB-exposed males. Computational analysis also demonstrated enhanced AHR and liver-X-receptor (LXR) activation (higher *z*-scores) in PCB-exposed females vs. males. With regards to gut microbiome, both exposure and sex impacted the composition of microbial communities. Intriguingly, only PCB-exposed males exhibited increased *Dehalobacterium* abundance, and decreased mRNA levels for genes encoding gut barrier and antimicrobial proteins (*Ocln*, *Reg3g*). Overall, PCB-exposed females exhibited an altered proteome relevant to AHR and LXR responses, while PCB-exposed males exhibited more distinct changes in gut microbiota coupled with altered ileal gene expression. The findings suggest that, in addition to biological sex, organ-organ interactions should be considered when predicting toxicity outcomes, particularly for persistent compounds such as PCBs that can impact multiple organs simultaneously yet have tissue-specific toxic effects.

Keywords PCBs, Sex differences, Liver, Microbiome, Proteomics

Abbreviations

AHR	Aryl hydrocarbon receptor
CAMP	Cathelicidin antimicrobial peptide
CAR	Constitutive androstane receptor
Cldn	Claudin
CYP	Cytochrome P450
DE	Differentially expressed
EGFR	Epidermal growth factor receptor
ER	Estrogen receptor
FCON	Female controls
FGF15	Fibroblast growth factor 15

[1]Center for Cardiometabolic Science, University of Louisville, Louisville, KY 40202, USA. [2]KY INBRE Bioinformatics Core, University of Louisville, Louisville, KY 40202, USA. [3]Department of Medicine, Division of Gastroenterology,, University of Louisville School of, Medicine Hepatology & Nutrition, Kosair Charities Clinical and Translational Research Building, 505 S. Hancock St., Louisville, KY 40202, USA. [4]Center for Integrative Environmental Health Sciences, University of Louisville, Louisville, KY 40202, USA. [5]Department of Pharmacology & Toxicology, School of Medicine, University of Louisville, Louisville, KY 40202, USA. [6]The Hepatobiology and Toxicology Center, University of Louisville, Louisville, KY 40202, USA. [7]Kidney Disease Program and Clinical Proteomics Center, University of Louisville, Louisville, KY 40202, USA. [8]Department of Bioinformatics and Biostatistics, School of Public Health and Information Sciences, University of Louisville, Louisville, KY 40202, USA. [9]Biostatistics Shared Facility, James Graham Brown Cancer Center, School of Medicine, University of Louisville, Louisville, KY 40202, USA. [10]Superfund Research Center, University of Louisville, Louisville, KY 40202, USA. ✉email: banrida.wahlang@louisville.edu

FMO	Flavin-containing monooxygenase
FPCB	Female PCBs
LDA	Linear discriminant analysis
LEFSE	Linear discriminant analysis Effect Size, LXR, liver-X-receptor
MCON	Male controls, miR, micro RNA
MPCB	Male PCBs
MUC	Mucin
OCLN	Occludin
OTUS	Observed taxonomic units
PCBS	Polychlorinated biphenyls
PXR	Pregnane-xenobiotic receptor
TASLD	Toxicant-associated steatotic liver disease
TASH	Toxicant-associated steatohepatitis
TCDD	2,3,7,8-Tetrachlorodibenzo-*p*-dioxin
Tff3	Trefoil factor 3
Tjp1	Tight junction protein 1
TMT	Tandem mass tag

Health concerns pertinent to environmental pollutants, including exposures to polychlorinated biphenyls (PCBs), continue to intensify in the field of environmental health as global industrialization flourishes. PCBs are anthropogenic environmental toxicants, originally manufactured for industrial purposes and subsequently banned from production and usage when their carcinogenic properties were reported[1]. While one of the predominant and commonly known health effects associated with these legacy forever chemicals is cancer, other less severe but more chronic effects such as cardiometabolic diseases have also been acknowledged[2,3]. Notably, associations between PCB exposures and steatotic liver disease, hypertension, and diabetes have been substantiated in numerous epidemiologic and toxicological studies[4–7].

Despite production being halted for decades now, PCBs still remain in our environment due to their recalcitrant nature towards both degradation and metabolism[8]. PCBs are still detected in the American population as documented in the National Health and Nutrition Examination Survey (NHANES) studies with heavily chlorinated PCB congeners having higher detection levels[9]. These polyhalogenated organic compounds are broadly classified as coplanar or non-coplanar congeners, based on the degree of chlorination on the biphenyl ring. Structure-activity relationships conferred coplanar congeners as activators of the aryl hydrocarbon receptor (AHR), similar to 2,3,7,8-Tetrachlorodibenzo-*p*-dioxin (TCDD) and hence also known as "dioxin-like" PCBs[10]. In contrast, non-coplanar PCBs are better activators of the constitutive androstane receptor (CAR) and often referred to as "non-dioxin-like" or phenobarbital-like PCBs[11]. Previously, our research group have demonstrated how dioxin and non-dioxin like PCBs can elicit differential effects on the liver and other metabolic parameters depending on the dose and duration of exposure[12–14]. Importantly, our studies also highlighted the significance of accounting for sex differences with PCB exposures as these toxicants implicitly act as both metabolism and endocrine-disrupting chemicals[15]. Indeed, female mice acutely exposed to a mixture of dioxin-like and non-dioxin-like PCBs manifested greater susceptibility to steatotic liver disease and impaired glucose uptake compared to exposed males[16].

Steatotic liver disease is a spectrum of liver pathologies, initially manifested by accumulation of lipid droplets in the liver (steatosis), which may be accompanied by inflammation (steatohepatitis). If left untreated, steatohepatitis can further progress to fibrosis and cirrhosis, and ultimately hepatocellular carcinoma and fulminant liver failure. Steatotic liver disease is either a risk factor for other metabolic complications such as diabetes, obesity and cardiovascular diseases or occurs in parallel with one or more of these complications[17]. Multiple mechanisms with regards to PCBs' contribution to steatotic liver disease and to an extent, glucose intolerance and diabetes, have been postulated. Primarily, PCBs have been shown to interact with hepatic xenobiotic and endobiotic receptors to elicit changes in the hepatic transcriptional machinery leading to downstream effects on hepatic lipid and carbohydrate metabolism[7,18,19]. Further, PCBs can also interact with nuclear receptors including thyroid and sex hormone receptors, resulting in endocrine dysfunction and disruption of overall energy homeostasis[20]. In addition, PCBs can induce oxidative and endoplasmic reticulum stress and trigger inflammatory responses through interactions with NF-KB, among other means[4,21]. PCBs can also inhibit key phosphoproteins in the liver and interrupt physiological phosphorylation processes leading to hepatic signaling disruption[22,23].

More recently, other novel mechanisms identified for PCB contributions to steatotic liver disease include PCB-induced RNA modifications in the liver (hepatic epitranscriptome) resulting in changes in hepatic transcript levels for key genes regulating energy metabolism[24,25]. Another increasingly recognized mechanism is PCB effects on gut microbiota and intestinal function that can impact liver health and function, in part, through the gut-liver axis[7,26,27]. However, all these mechanistic toxicologic studies were performed majorly in male experimental models and there is a lack of understanding on how these biological events pan out in females. To address this knowledge gap, the current study aims to identify sex differences in the hepatic proteome and gut microbiome, and assess how biological sex impact PCB responses, in order to gain insight on sex-specific liver proteins and gut parameters impacted by PCB exposures. This comprehensive molecular profiling will also provide information on sex-specific pathways that potentially play a role in driving distinct PCB toxicity outcomes in males versus females. To achieve this objective, the current study adopts a holistic, multi-omic approach using liver and intestinal samples obtained from a previously characterized acute exposure mouse study[16] with verified sex-specific phenotypic outcomes, in part, to ensure validity of the study purpose and objective.

Materials and methods

Animal model

The mouse exposure study was approved by the University of Louisville Institutional Animal Care and Use Committee (IACUC) under Protocol # 14077. The UofL IACUC assumes responsibility for those functions given in the National Research Council Guide for the Care and Use of Laboratory Animals, the NIH Public Health Service Policy on Humane Care and Use of Laboratory Animals, and the Animal Welfare Act. Thus, all animal experiments were performed in accordance with the National Research Council Guide for the Care and Use of Laboratory Animals. Further, the animal experiments and data reporting are in compliance with the ARRIVE guidelines. Male and female C57Bl/6 mice (7–8-week-old) were obtained from The Jackson Laboratory (Bar Harbor, ME) and housed in a temperature- and light- controlled room (12 h light; 12 h dark) with food and water *ad libitum*. Five mice were housed per cage in this 2-week study. All animals were fed a low-fat, synthetic diet consisting of 20.0%, 69.8%, and 10.2% of total calories from protein, carbohydrate, and fat respectively (TD06416, Envigo, Indianapolis, IN) throughout the study period. Mice were randomly divided into four groups (n=10, total=40) based on sex and exposure utilizing a 2X2 design (Male-CON, Male-PCB, Female-CON, Female-PCB), On week 0, mice were allowed to acclimate to the new facility. At the beginning of week 1, vehicle control (corn oil) or a mix of PCBs (purchased from AccuStandard, CT) solubilized in corn oil was administered to mice by oral gavage. The PCB mix comprised of the commercial PCB mixture, Aroclor 1260 (20 mg/kg) which constitutes a higher proportion of non-dioxin-like and heavily chlorinated PCB congeners, and the classic dioxin-like congener, namely PCB126 (10 µg/kg). At the beginning of week 2, a second dose of PCB126 (10 µg/kg) or vehicle control was administered to mice via oral gavage. Repeated dosing for PCB 126 was performed because, as opposed to the heavily chlorinated congeners in Aroclor 1260 which are highly resistant to metabolism, PCB 126 is less chlorinated and can be metabolized in the liver. Thus, the repeated dosing will ensure that the parent compound effect is sustained in the two-week study. At the end of week 2, mice were euthanized using ketamine/xylazine (100/20 mg/kg body weight, i.p.) and samples collected for further analysis. A schematic diagram depicting the experimental design, timeline, dosing regimen and downstream analyses is provided in Supplemental Fig. S1.

Dose rationale

The PCB doses utilized in the current study were designed to mimic current PCB bioaccumulation patterns in humans and routinely used by our group in PCB exposure mouse models[16,18]. The congener composition in Aroclor 1260 also strongly resemble human PCB bioaccumulation patterns[11]. Circulating levels of PCBs (lipid-adjusted) reported in measurements from NHANES participants and PCB-exposed populations such as the Anniston Community Health Survey (ACHS) range from around 70 to 170 ng/g[9,28,29]. The National Toxicology Program (NTP) has also performed extensive studies on PCB tissue distribution in rodents in 2-year gavage studies and demonstrated that PCB levels in the liver were approximately 10 times higher than lipid-adjusted serum levels, irrespective of the dose administered or exposure duration[30]. Based on extrapolations from these NTP studies, a 20 mg/kg cumulative dose of Aroclor 1260 would result in serum PCB levels at approximately 170 ng/g and liver PCB tissue levels at around 3000 ng/g. Thus, the Aroclor 1260 dose is expected to yield serum PCB levels similar to those measured in the ACHS participants. With regards to PCB 126, exposures by total PCB mass to dioxin-like PCBs including PCB 126 is >0.1% of the total PCB exposures in NHANES participants[9], reflective of the cummulative dose of the 20 µg/kg (0.1% of Arcolor 1260) used in the study.

Proteomics

Protein samples (n=5) were extracted from mouse livers in 1% SDS modified RIPA buffer using bead homogenization. To avoid cage effects, mouse livers were selected randomly for each group but ensuring that at least two liver samples of a group came from animals housed in a different cage than the other three samples of that same group. Protein concentrations were measured using Pierce™ BCA Protein Assay Kit (Thermo Fisher Scientific, Waltham, MA) according to the manufacturer's instructions. Protein lysates (200 µg) were trypsinized using the modified filter-aided sample preparation method. Firstly, protein samples were reduced and denatured using dithiothreitol and 8 mol/L urea, respectively, and alkylated using iodoacetamide. This was followed by centrifugation through a high molecular weight cutoff centrifugal filter (Millipore Sigma, 10k MWCO) and subsequent overnight digestion with sequencing grade trypsin (Promega, Madison, WI, USA) at 37 °C. The digested peptides were collected and cleaned with a C18 Proto™ 300 Å ultra microspin column. Digested peptide samples (50 µg) were then labeled with tandem mass tag (TMT) TMT10plex™ isobaric label reagent set (Thermo Fisher Scientific). Labeled samples were concentrated and desalted with Oasis HLB extraction cartridges (Waters Corporation, Milford, MA) using a modified protocol for extraction of the digested peptides. Next, samples were then separated by high pH reversed phase separation with fraction concatenation on a Beckman System Gold LC system supplemented with 126 solvent module and 166 UV–Vis detector in tandem with a BioRad Model 2110 Fraction Collector. Liquid chromatography/mass spectrometry was used to measure TMT-labeled peptides. Briefly, every high pH reversed phase fraction was dissolved in 50 µL solution of the combination of 2% v/v acetonitrile with 0.1% v/v formic acid. 1 µL of each fraction was analyzed on EASY-nLC 1000 UHPLC system (Thermo Fisher Scientific) and an Orbitrap Elite–ETD mass spectrometer (Thermo Fisher Scientific). The raw spectral data obtained from the mass spectrometer were analyzed using Proteome Discoverer (2.5.0.400 Settings).

Proteomic analysis

Statistical analyses of the proteomic data were performed using R software. Proteins exhibiting 40% or more missing values were excluded from the analysis, which resulted in 3837 proteins out of 4533 identified. All 3837 proteins showed complete observations in all 20 samples and no imputation on missing values was needed.

Quantile normalization method was then conducted on the complete dataset across different groups using the function "*normalize.quantiles*" in R package "*preprocessCore*"[31]. Subsequently, the data were analyzed using linear models, with sex and exposure as the main effects, and the response variable being the log-transformed expression data (base 2). Contrasts using moderated *t*-tests were generated to explore exposure effect (PCB vs. control) for each sex, sex difference for each exposure group, as well as the interaction between exposure and sex using "*Limma*" package[32]. The results were reported as mean expression levels, log fold-change (FC), *p*-value, and *p*-value adjusted by the Benjamini-Hochberg (BH) method to control the false discovery rate (FDR)[33]. As this was a discovery-based, high throughput analysis, the FDR was set at <0.1, and the unadjusted *p*-value were also provided. Computational analyses on significantly altered proteins for each comparison group (up-regulated proteins at $\log_2$ FC ≥0.5, down-regulated proteins at $\log_2$ FC ≤−0.5, along with adjusted *p*-value <0.10) were performed using MetaCore (Clarivate Analytics). Briefly, the protein lists for each comparison group which included both upregulated and downregulated proteins along with the respective fold change were uploaded to MetaCore. Analyses including "GO Process", "Interaction by Protein Function", "Enrichment by Diseases (by Biomarkers)" and "Enrichment by Pathway Maps" were performed for each comparison group using "One-click Analysis" with parameters set at *p*-value <0.05 and FDR <0.05.

16S rRNA sequencing

Microbial genomic DNA was extracted from mouse cecal samples (n=10) using the DNeasy PowerSoil Pro Kit (Qiagen, Germantown, MD) according to the manufacturer's instruction. Illumina MiSeq technology targeting the variable V3 and V4 regions of 16S ribosomal RNA was used to determine cecal bacterial composition. Libraries were prepared using Illumina's 16S library preparation guide and Illumina's Nextera Index Kit (FC-121–1012). Briefly, quantitation of microbial genomic DNA was performed using Qubit Broad Range (BR) assay (Thermo Fisher Scientific) in a Qubit 2.0 Fluorometer. Amplicon PCR was carried out using primers that were complementary upstream and downstream of the region of interest with overhang adapters. The 16S variable region was amplified using 12.5 ng of microbial genomic DNA and Amplicon PCR Clean-Up carried out using AMPure XP beads. Index PCR was then performed to attach dual indices and Illumina sequencing adapters using the Nextera XT Kit (FC-121–1012). Following the Index PCR Clean-Up using SpriSelect beads, sequencing libraries were aliquoted and mixed to make pooled libraries and concentrations determined on the Bioanalyzer. Next, after normalization, the pooled library was denatured and mixed with the PhiX control library. Sequencing was done on a Nano-300 cycle test chip (MS-103–1001) to confirm sample concentration followed by Illumina MiSeq Reagents kit v3 (600 cycles) (MS-102–3003) at 10 pM and 30% PhIX.

16S rRNA metagenomics analysis

The microbial diversity analysis and taxonomic profiling were conducted using Quantitative Insights into the Microbial Ecology (QIIME) version 2–2022.2.2[34]. The pipeline utilized for bioinformatics analysis is described as follows: i) Quality control of the 40 raw sequences FASTQ files was performed using FastQC version 0.10.1[35], ii) Demultiplexed sequence reads were imported to QIIME2-2022.2, and trimming was performed to remove low-quality data using the parameters p-trunc-len-f 270 and p-trunc-len-r 220. These trimming thresholds were selected after examining the interactive quality plots (Supplemental Fig. S2) to ensure that high quality sequence regions were retained while still maintaining sufficient overlap between paired-end reads, iii) Denoising of reads into amplicon sequence variants (ASVs) was performed using DADA2 QIIME2-2022.2 plugin[36], iv) Taxonomic classification of ASVs was done using VSEARCH qiime2-2022.2 plugin at similarity cutoff value at 97% followed by mapping of ASVs using Greengenes 13_8_99-nb classifier[37], v) Phylogenetic tree was constructed using QIIME phylogeny align-to-tree-mafft-fasttree algorithm. For data rarefaction, it was determined that the smallest and largest number of read counts are 12,698 and 47,091, respectively (Supplemental Table S1). Based on the alpha rarefaction curves (Supplemental Fig. S3), the sequence sampling depth of 23, 192 was utilized when generating all alpha and beta diversity core metrics results. The Faith's PD curve for M-CON-4 (12,698 reads) did not reach saturation at this depth, whereas rarefaction curves for all other samples plateaued above 20,000 reads. To avoid compromising diversity and taxonomic assessment, this sample was excluded from further analysis. In addition, this sample showed low reverse strand sequencing quality. After removal, the control group retained nine samples, which was sufficient for statistical power, and therefore all subsequent analyses were conducted without this sample. Beta diversity PERMANOVA analyses were performed using the QIIME2 pipeline, and principal component analysis plots were generated using Partek Flow 11.0.24.0414. To account for any potential cage effect, an additional PERMANOVA analysis using adonis2 function in R, which allows inclusion of "cage" as a covariate, was performed. Alpha diversity output obtained from QIIME2 was visualized and analyzed using the Kruskal Wallis test with Dunn multiple correction in GraphPad PRISM Version 10.4.2. Taxonomic data was represented as bar plots using GraphPad PRISM version 10.4.2, heatmaps using Partek genomics suite version 7.21.1119, and analyzed using the Kruskal Wallis test with Bayesian q-value correction[38]. Linear discriminant analysis Effect Size (LEfSe) was used to identify the enrichment profile of taxa characterizing the differences between the experimental groups[39]. Analysis was performed on family and genus relative abundance data using Huttenhower Lab Galaxy Server 2.0. Significant enrichment of taxa was calculated via a series of Kruskal Wallis non-parametric tests to determine the presence of significant alterations in taxonomic abundance between groups (adjusted p <0.05). This was followed up using linear discriminant analysis to estimate the effect size of any significant alterations set at linear discriminant analysis (LDA) cutoff score >2 and p <0.05.

RT-PCR and western blot analysis

Total RNA was extracted from mouse ileal samples (n=10) with RNA-STAT 60 (Tel-Test, Austin, TX) using bead homogenization. RNA purity and quantity was assessed with the NanoDrop One (Thermo Fisher Scientific) and cDNA was synthesized from total RNA using qScript cDNA Synthesis Kit (Quantabio, Beverly, MA).

RT-PCR was performed on the CFX384 TM Real-Time System (BioRad, Hercules, CA) using iTaq Universal Probes Supermix and Taqman probes purchased from Thermo Fisher Scientific (Supplemental Table S2). Four housekeeping genes were tested and stability analyzed using RefFinder[40], a web-based comprehensive tool for screening reference genes by integrating four computational programs (geNorm, NormFinder, BestKeeper, and the comparative ΔCt method). For the current study, *Ppia* was identified as the most stable housekeeping gene from the four tested (Supplemental Fig. S4). Gene expression levels were calculated according to the $2^{-\Delta\Delta Ct}$ method. The levels of mRNA were normalized relative to the levels of the housekeeping gene (*Ppia*) and mean expression levels in unexposed, male mice were set at ~1.

Liver tissue was homogenized in RIPA Buffer, supplemented with protease, and phosphatase inhibitors (Sigma-Aldrich, St. Louis, MO) to obtain protein samples for western blot analysis (n=6). Protein concentration was determined by Pierce™ BCA Protein Assay Kit (Thermo Fisher Scientific). Protein (30 µg) was separated on a 4–15% gradient SDS Gel (BioRad, Hercules, CA), transferred, blocked, and incubated with primary antibody according to the manufacturer's instructions. The membranes were incubated in Pierce™ ECL agents (Thermo Fisher Scientific) and luminescent signals were captured with BioRad Chemidoc Imaging System. Western blot bands were quantified using BioRad Image Software. Primary antibody for CYP1A2 (D2V75) was obtained from Cell Signaling Technology (Danvers, MA, USA), CD36 (ab133625) and flavin monooxygenase 3 (FMO3, ab126711) from Abcam (Cambridge, MA, USA), and Actin (A5441) from Millipore Sigma (St. Louis, MO).

Additional statistical analyses

Graphs were plotted using GraphPad Prism 10.4.2 (GraphPad Software Inc., La Jolla, CA, USA) unless specified otherwise. Western blot and gene expression data were analyzed by two-way ANOVA, for two factors, namely "Sex" and "PCBs" and their interactions in GraphPad Prism 10.4.2. This was followed by multiple comparison tests with Bonferroni correction for sub-group analyses (adjusted $p < 0.05$ was considered statistically significant). In the event of high data variability in a group, an outlier test was performed using the ROUT method with false discovery rate (FDR) set at 0.1 %. In terms of reporting the findings, based on the research objective and study design, basal sex differences were reported first, followed by PCB effects.

Results

Effects of biological sex and PCB exposure on the hepatic proteome

A total of 3837 hepatic proteins were analyzed after adjustment for missing values with the exposed male versus female group showing the greatest number of differentially expressed (DE) proteins among all comparison groups (Fig. 1A, B & C). A principal component analysis of the normalized dataset was also performed to visualize the distinct proteomic profiles between groups (Fig. 1D). While biological sex was a major driver for the DE proteins observed (44 upregulated and 41 downregulated in MCON vs. FCON), PCB exposure further increased the number of DE proteins between males and females (61 upregulated and 82 downregulated in MPCB vs. FPCB). PCB exposure within each sex however resulted in relatively modest changes (8 upregulated in MCON vs. MPCB and 3 upregulated in FCON vs. FPCB). A list of the top ten DE proteins for each comparison group is shown in Table 1 and a list of all DE proteins for each comparison group is presented in Supplemental ExcelTable 1. Notably, there were no similar DE proteins identified between all 4 comparison groups (Table 1 and Fig. 1E). Nonetheless, 66 common DE proteins were identified in both the MCON vs. FCON and MPCB vs. FPCB groups including flavin-containing monooxygenase 3 (FMO3) and cytochrome P450 enzymes such as CYP2A4. Only 2 common DE proteins were identified in both MCON vs. MPCB and FCON vs. FPCB groups, namely CYP1A1 and CYP1A2. Unique DE proteins identified in the MCON vs. MPCB group included CYP2B19, CYP4A10, CYP2A5, CYP2C29, CYP5A and retinol-binding protein 4 (RBP4). Only one unique DE protein was observed in the FCON vs. FPCB group, namely HIV-1 tat interactive protein 2 (HTATIP2), an oxidoreductase.

To validate the proteomic findings, western blot analysis of selected DE proteins including FMO3 (upregulated in both female groups), CYP1A2 (upregulated in both PCB groups) and CD36 (upregulated only in the exposed female group vs. the exposed male group) was performed. Importantly, CD36 is involved in hepatic lipid uptake and its upregulation is implicated in steatotic liver development[41]. In concordance with the proteomic results, protein expression of FMO3 was increased in both the female groups with and without exposure (Fig. 2A and Supplemental Fig. S5) with two-way ANOVA reporting a significant sex effect. Exposed females also exhibited a trend towards significance for higher FMO3 expression vs. their sex-matched controls (p=0.051), potentially reaffirming the proteomic findings wherein the MPCB vs. FPCB group displayed higher FMO3 fold induction than MCON vs. FCON. In contrast to FMO3, CYP1A2 expression was upregulated only in PCB-exposed groups, regardless of sex (Fig. 2B and Supplemental Fig. S5) with two-way ANOVA reporting a significant PCB effect. Lastly, CD36 protein expression was largely driven by sex, and this difference was more pronounced in the exposed male vs. exposed female groups (Fig. 2C and Supplemental Fig. S5). Nonetheless, exposed females also showed a trend towards significance for increased CD36 protein expression levels (p=0.054), compared to their sex-matched controls. Overall, the data from the western blot analysis aligned with the proteomic output results.

Pathway analysis for differentially expressed proteins and identification of sex-specific enriched pathways

To identify key biological processes and pathways impacted by changes in hepatic proteins for each comparison group, downstream computational enrichment analyses were performed using MetaCore. With regards to "GO Processes", similar biological processes were affected in the MCON vs. FCON and MPCB vs. FPCB groups including metabolic and catabolic processes, xenobiotic responses, lipid synthesis and breakdown, and carbohydrate and protein processes (Fig. 3). These results highlighted basal sex differences in energy metabolism particularly for fatty acid synthesis and oxidation. Processes enriched only in the PCB-exposed male and female groups included "omega-hydroxylase P450 pathway", "dibenzo-p-dioxin metabolic process", "hepatocyte

A

Comparison	MCON vs. FCON		MPCB vs. FPCB		MCON vs. MPCB		FCON vs. FPCB	
Summary of results	*p*-Not Adj	*p*-Adj	*p*-Not Adj	*p*-Adj	*p*-Not Adj	*p*-Adj	*p*-Not Adj	*p*-Adj
Proteins analyzed	3837	3837	3837	3837	3837	3837	3837	3837
DE proteins	323	73	634	146	157	8	52	3
DE proteins (-0.5 <log_2FC <0.5)	182	6	369	34	97	0	34	0
Up-regulated proteins ($log_2FC \geq 0.5$)	78	44	147	61	36	8	11	3
Down-regulated proteins ($log_2FC \leq$-0.5)	63	41	118	82	24	0	7	0

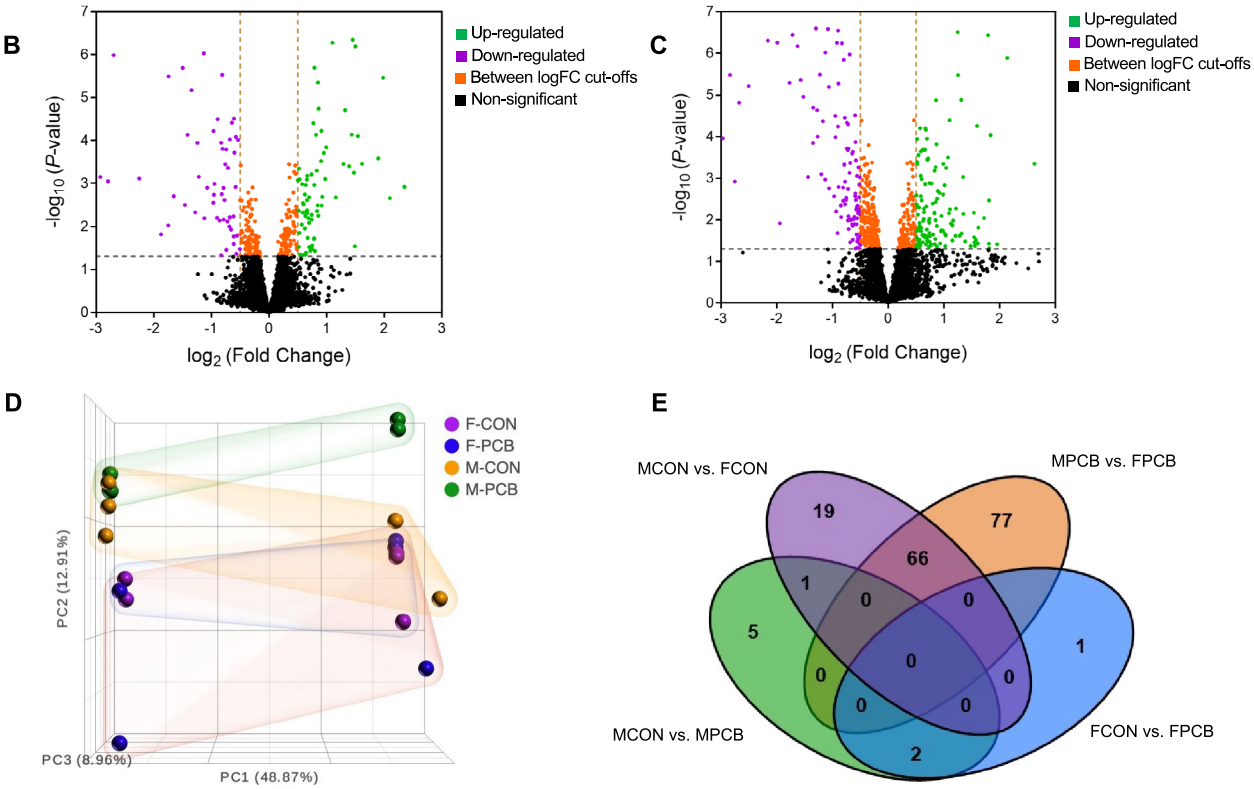

Fig. 1. Effect of sex and PCBs on the hepatic proteome. (**A**) A summary table of the overall results is presented. Proteins exhibiting 40% or more missing values were excluded from the analysis, which resulted in 3837 proteins being analyzed out of 4533 identified. The number of differentially expressed (DE) proteins was obtained for each comparison group. *p*-Not Adj is p <0.05 and *p*-Adj is p <0.1, after correcting for false discovery rate. FC - fold change. Volcano plots were generated to graphically depict alterations in hepatic proteins for (**B**) MCON vs. FCON and (**C**) MPCB vs. FPCB. (**D**) Principal component (PCA) analysis of the normalized raw proteomic data was performed and a PCA plot generated. (E) A Venn diagram showing the number of shared or unique DE proteins based on the four comparison groups was constructed.

differentiation" and metal processes. Processes identified in all 4 groups included hormone processes such as regulation of hormone levels, implicating that both sex and PCBs may modulate these endpoints. Additional analysis, namely "Enrichment by Pathway Maps" was performed for the PCB-exposed groups and the top 10 enriched pathways shown in Table 2. Pathway enrichment analysis demonstrated that while in males, "aryl hydrocarbon receptor signaling pathway" was the top enriched pathway, "estradiol metabolism" was the topmost enriched pathway in females. PCB exposure in males and females however enriched similar pathways related to "dioxin-like" chemicals and primarily driven by CYP1A1 and CYP1A2 upregulation.

Interaction by protein function analysis and disease enrichment

To better assess protein activity and function based on DE proteins for each group, "Interaction by Protein Function" analysis was performed in MetaCore (Fig. 4A). Transcription factors were the major output from this analysis, while enzymes, co-activators and to an extent, micro-RNAs, were also identified. In terms of xenobiotic receptors, AHR showed the highest activity (by *z*-score), and this was observed only in the MPCB vs. FPCB and FCON vs. FPCB comparison groups, suggesting that AHR activation was predominant in the exposed female group. Surprisingly, CAR and pregnane-xenobiotic receptor (PXR) activity were observed only in the MCON vs. FCON and MPCB vs. FPCB groups. For endobiotic receptors, liver-X-receptor (LXR)-alpha activity was observed only in the MCON vs. MPCB and FCON vs. FPCB with the latter group showing a higher *z*-score,

Accession number	Description/protein name	Log_2FC	*p*-Not Adj	*p*-Adj
MCON vs. FCON				
P97501	Flavin-containing monooxygenase 3, GN=Fmo3	3.7812	0E-04	0E-04
P15392	Cytochrome P450 2A4, GN=Cyp2a4	3.3609	0E-04	0E-04
P12790	Cytochrome P450 2B9, GN=Cyp2b9	2.3984	0E-04	0E-04
Q9QYR7	Acyl-coenzyme A thioesterase 3, GN=Acot3	2.2152	0E-04	0E-04
G3X982	Aldehyde oxidase 3, GN=Aox3	−1.2621	0E-04	0E-04
P11714	Cytochrome P450 2D9, GN=Cyp2d9	−2.0058	0E-04	0E-04
Q8K182	Complement component C8 alpha chain, GN=C8a	−2.0154	0E-04	0E-04
Q5FW60	Major urinary protein 20, GN=Mup20	−2.3071	0E-04	0E-04
P19157	Glutathione S-transferase P 1, GN=Gstp1	−2.4968	0E-04	0E-04
Q91WL5	Cytochrome P450 4A12A, GN=Cyp4a12a	−2.9727	0E-04	0E-04
MPCB vs. FPCB				
P97501	Flavin-containing monooxygenase 3, GN=Fmo3	4.1401	0E-04	0E-04
P15392	Cytochrome P450 2A4, GN=Cyp2a4	3.5552	0E-04	0E-04
Q9QYR7	Acyl-coenzyme A thioesterase 3, GN=Acot3	2.2881	0E-04	0E-04
P56657	Cytochrome P450 2C40, GN=Cyp2c40	1.7782	0E-04	0E-04
P12790	Cytochrome P450 2B9, GN=Cyp2b9	1.6760	0E-04	0E-04
Q63880	Carboxylesterase 3 A, GN=Ces3a	−1.0799	0E-04	0E-04
P28665	Murinoglobulin-1, GN=Mug1	−1.1592	0E-04	0E-04
Q9DBW0	Cytochrome P450 4V2, GN=Cyp4v2	−1.2969	0E-04	1E-03
G3X982	Aldehyde oxidase 3, GN=Aox3	−1.3964	0E-04	0E-04
Q8BH35	Complement component C8 beta chain, GN=C8b	−1.9306	0E-04	0E-04
MCON vs. MPCB				
P00186	Cytochrome P450 1A2, GN=Cyp1a2	3.3404	0E-04	0E-04
P00184	Cytochrome P450 1A1, GN=Cyp1a1	3.1634	0E-04	0E-04
O55071	Cytochrome P450 2B19, GN=Cyp2b19	3.9063	0E-04	8.2E-03
O88833	Cytochrome P450 4A10, GN=Cyp4a10	0.8384	0E-04	8.2E-03
P20852	Cytochrome P450 2A5, GN=Cyp2a5	1.7485	0E-04	9.7E-03
Q64458	Cytochrome P450 2C29, GN=Cyp2c29	2.0350	0E-04	1.25E-02
P56395	Cytochrome b5, GN=Cyb5a	0.8788	0E-04	2.21E-02
Q00724	Retinol-binding protein 4, GN=Rbp4	0.7441	1E-03	3.55E-02
FCON vs. FPCB				
P00186	Cytochrome P450 1A2, GN=Cyp1a2	3.0604	0E-04	0E-04
P00184	Cytochrome P450 1A1, GN=Cyp1a1	2.4387	0E-04	0E-04
Q9Z2G9	Oxidoreductase HTATIP2, GN=Htatip2	1.3564	0E-04	2.83E-02

Table 1. The top ten differentially expressed (DE) proteins based on ascending adjusted *p*-values for each comparison are presented. The first experimental group mentioned in each comparison serves as the reference group. Note: Accession number is based on UniProt Protein ID. Significance is set at $p < 0.05$ for unadjusted and $p < 0.10$ for adjusted. Abbreviation: GN, gene name; FC, fold change.

while peroxisome proliferator-activated receptor alpha (PPAR alpha) activity was observed in all comparison groups except in the FCON vs. FPCB group. Furthermore, for most hormone receptors, protein activity was only observed in the MCON vs. FCON and MPCB vs. FPCB groups. Likewise, for other transcription factors including hepatocyte nuclear factors, protein activity was only observed in the MCON vs. FCON and MPCB vs. FPCB groups. Significantly, APOB activity was observed only in the MPCB vs. FPCB group. However, with regards to micro-RNAs, activity for multiple microRNAs, including the liver specific miR-122-5p, was observed only in the FCON vs. FPCB group.

In addition to protein function, disease enrichment analysis was also performed to identify if differences in the protein landscape can modulate disease endpoints. Selected diseases including liver, intestinal, cardio-metabolic, and hormone-related diseases were examined (Fig. 4B). In general, "liver diseases" was enriched in all 4 comparison groups while only the MCON vs. MPCB and FCON vs. FPCB showed enrichment for "chemical and drug-induced liver injury". Further, only the MPCB vs. FPCB group showed enrichment for "fatty liver". "Intestinal diseases" were enriched only in the MCON vs. FCON and MPCB vs. FPCB groups while "endocrine system diseases" were enriched only in the MCON vs. MPCB and FCON vs. FPCB.

Effects of biological sex and PCB exposure on gut bacterial diversity

The 16S rRNA gene sequencing was performed to determine the sex-specific PCB effects on the gut microbiome. Differences in microbial diversity within individual samples were evaluated using alpha diversity measures, and

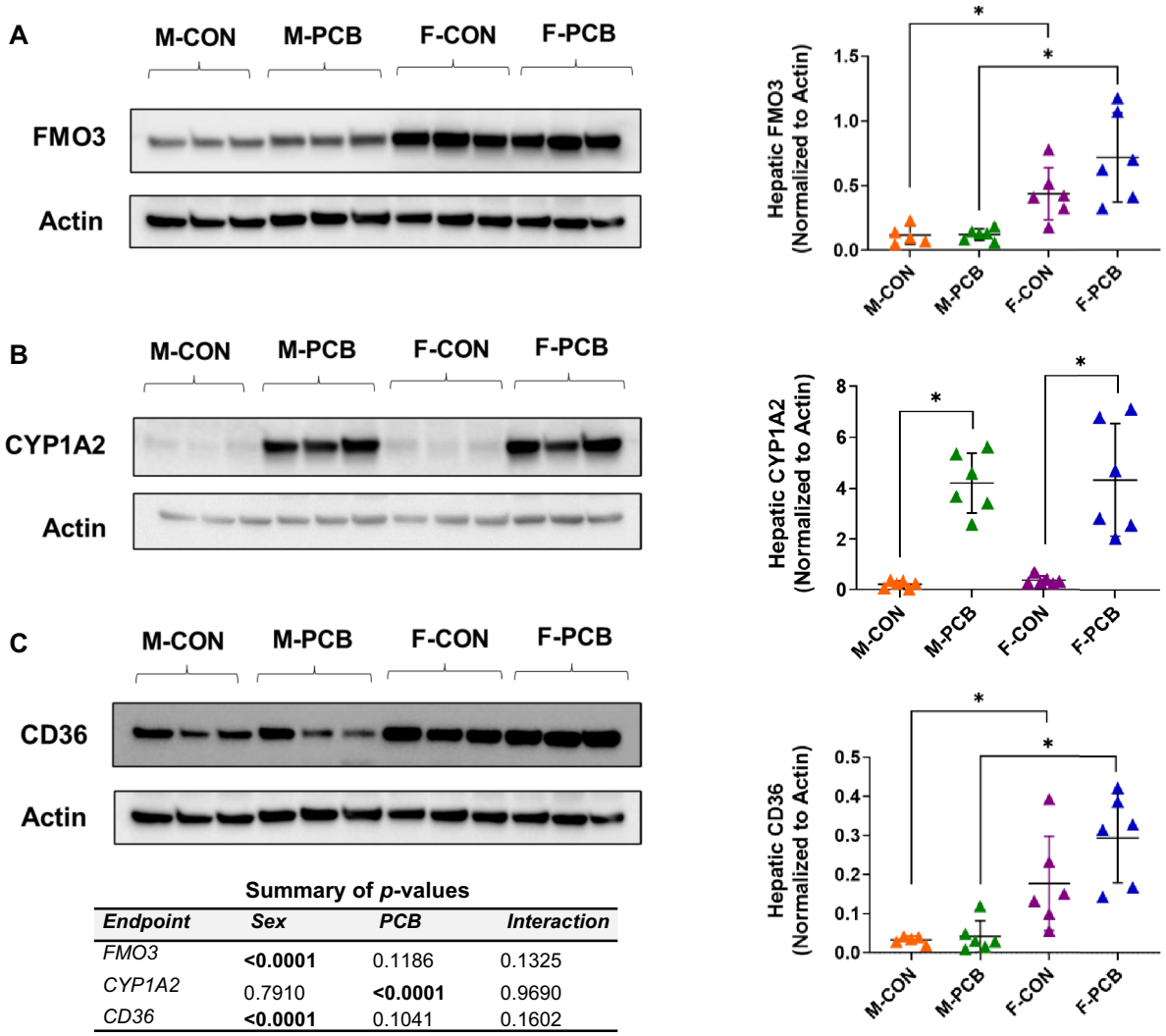

Summary of *p*-values

Endpoint	*Sex*	*PCB*	*Interaction*
FMO3	**<0.0001**	0.1186	0.1325
CYP1A2	0.7910	**<0.0001**	0.9690
CD36	**<0.0001**	0.1041	0.1602

Fig. 2. Validation of selected proteins using western blot analysis. Selected hepatic proteins that were significantly altered were further validated by Western blot analysis, namely (**A**) FMO3, (**B**) CYP1A2, and (**C**) CD36. Representative blots are shown. The densitometry ratios of the target protein to the corresponding control protein, Actin was calculated. Note: FMO3 and CD36 share the same Actin control. A list of *p*-values from the two-way ANOVA analysis is also provided. Values are mean ± SD, **p* <0.05.

differences in diversity between samples were accessed using beta diversity measures. Multiple diversity metrics were included to capture distinct aspects of microbial community structure (e.g., richness, evenness, phylogeny, and abundance), as is standard in exploratory microbiome studies. These different metrics offer unique and biologically relevant insights, in addition to providing complementary information and supporting a transparent and robust interpretation of the results.

Alpha diversity indices namely Observed Species which measures species richness within a group, and Shannon Index which measures species richness and evenness within a group, indicated a significant sex difference, with females showing lower alpha diversity than their male counterparts, irrespective of exposure (Fig. 5A). In contrast, the Pielou Index which measures evenness within a group, and Faith Phylogenetic Diversity (Faith_pd) which measures species evolutionary relatedness within a group, indicated no differences between the groups (Supplemental Fig. S6). Beta diversity indices namely Jaccard which measures compositional similarity between groups, and Bray Curtis which measures compositional dissimilarity between groups, revealed a significant compositional difference between all groups (Fig. 5B). Notably, these differences in composition between all groups remained significant after adjusting for cage effects (Supplemental Table S3). In comparison to Jaccard and Bray Curtis, UniFrac tests measures compositional relatedness between groups. Unweighted UniFrac which measures absence and presence of taxa, and Weighted which measures absence, presence, and abundance of taxa, both indicated a significant compositional difference between males and females irrespective of exposure (Supplemental Fig. S6). Overall, the diversity analyses reveal that alterations in microbial diversity were mainly due to sex differences. However, both exposure and sex had a significant effect on the composition of microbial communities that are distinctive between all groups.

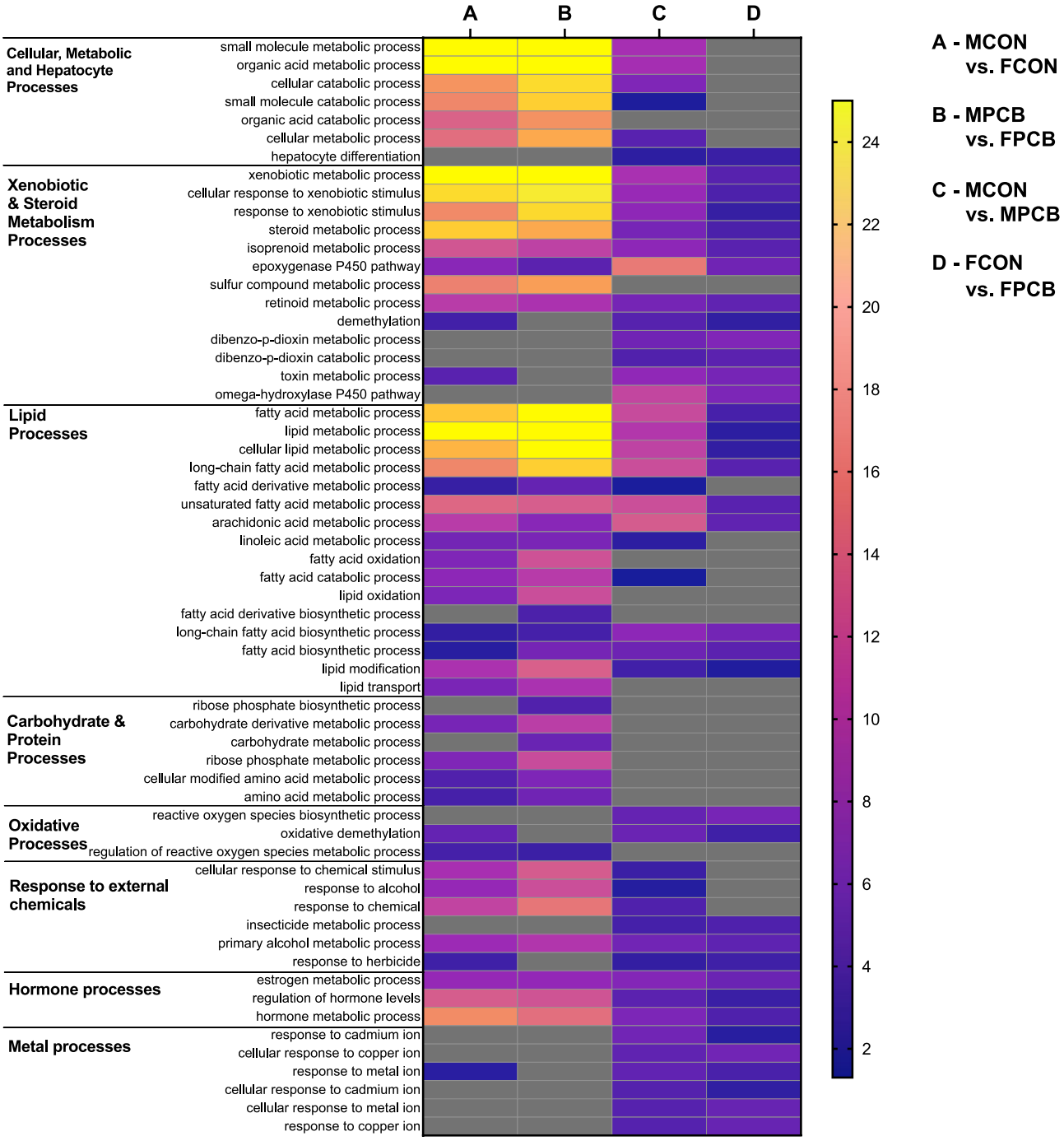

Fig. 3. Sex and PCB effects on gene ontology (GO) processes. A heat map showing different processes that were altered by sex and/or PCB exposures according to the -log(*p*-value) for each comparison. The first experimental group mentioned in each comparison serves as the reference group. The processes were obtained by GO analysis enrichment of the different proteins altered by sex and/or PCB exposures using MetaCore. A - MCON vs. FCON, B - MPCB vs. FPCB, C - MCON vs. MPCB, D - FCON vs. FPCB.

Sex and PCB exposure modulate gut bacterial abundance at higher taxa levels

Bacterial relative abundance at varying levels were further analyzed to identify the differences in microbial composition observed in the beta diversity analysis. At the phyla level (Fig. 6A and Supplemental Table S4), distinct sex differences were observed with females generally having lower abundance for Bacteroidetes, Proteobacteria and Tenericutes, and higher abundance for Actinobacteria, OD1, and Verrucomicrobia compared to males. However, in PCB-exposed females, there was only a significantly lower abundance for Tenericutes, and higher abundance observed only for Actinobacteria and OD1 (Parcubacteria) compared to exposed males. No significant alterations at the phyla level were observed in either males or females with PCB exposures.

Pathway maps	*p*-Value	FDR
MCON vs. MPCB		
Aryl hydrocarbon receptor signaling	8.063E-09	1.567E-07
Androstenedione and testosterone biosynthesis and metabolism p.1	8.706E-09	1.567E-07
Retinol metabolism	2.517E-08	3.020E-07
CAR-mediated direct regulation of xenobiotic metabolizing enzymes/Rodent version	8.972E-07	5.359E-06
CAR-mediated direct regulation of xenobiotic metabolizing enzymes/Human version	8.972E-07	5.359E-06
Estradiol metabolism	1.042E-06	5.359E-06
Benzo[a]pyrene metabolism	1.042E-06	5.359E-06
Acetaminophen metabolism	3.587E-06	1.614E-05
Naphthalene metabolism	5.376E-06	2.151E-05
Estrone metabolism	1.425E-04	5.130E-04
FCON vs. FPCB		
Estradiol metabolism	2.964E-05	1.641E-04
Benzo[a]pyrene metabolism	2.964E-05	1.641E-04
1-Naphthylamine and 1-Nitronaphtalene metabolism	3.408E-05	1.641E-04
Serotonin - melatonin biosynthesis and metabolism	3.563E-05	1.641E-04
Aryl hydrocarbon receptor signaling	4.742E-05	1.641E-04
Androstenedione and testosterone biosynthesis and metabolism p.1	4.924E-05	1.641E-04
2-Naphthylamine and 2-Nitronaphtalene metabolism	6.089E-05	1.679E-04
Acetaminophen metabolism	6.717E-05	1.679E-04
Retinol metabolism	8.303E-05	1.757E-04
Naphthalene metabolism	8.787E-05	1.757E-04

Table 2. The top ten enriched pathways along with the generated *p*-values and FDR values obtained from MetaCore using the "Enrichment by Pathway Maps" analysis for selected comparison groups.

Additionally, there was no change in dysbiosis index (Firmicutes/Bacteroidetes) between samples, indicating that neither sex nor exposure led to significant microbial dysbiosis.

Similarly, at the family level (Fig. 6B and Supplemental Table S5), 36 bacteria were identified with 17 significant alterations in abundance observed in the unexposed female versus male groups while 12 significant changes were observed in the PCB-exposed female versus male groups. Prominent observations include decreased abundance for *Bacteroidaceae* and *Staphylococcaceae* and increased abundance for *Clostridiaceae* and *Coriobacteriaceae* in unexposed females versus their male counterparts. However, these effects disappeared except for *Coriobacteriaceae* in PCB-exposed females versus their male counterparts. Notably, in PCB-exposed females, there was an increase in *Bifidobacteriaceae* and decreased *Ruminococcaceae* abundance compared to PCB-exposed males. Further, PCB effects at the family level were only observed in PCB-exposed males wherein PCB exposure resulted in an increased abundance for *Dehalobacteriaceae* and decreased abundance for *Bifidobacteriaceae* and *Leuconostocaceae* compared to their sex-matched controls.

Effects of sex and PCB exposure on gut bacterial abundance at lower taxa levels

At the genus level, 57 bacteria were identified, and 23 significantly altered bacterial abundance were observed in the unexposed female versus male group while only 15 were observed in the PCB-exposed female versus male group (Supplemental Table S6). These observations indicate that differences in microbial composition were mainly observed due to changes in sex as compared to PCB exposure.

To gain further insight on the effect size and distinguishing profiles between experimental groups at the genus level, LEfSe analysis was performed and LDA scores generated (Fig. 6C). The genus Bacteroides showed the largest difference in the unexposed mice, with males having higher abundance for *Bacteroidetes*, in addition to *Staphylococcus*, *Oscillospira*, *Anaerotruncus*, *Anaeroplasma*, *Solibacillus* and *Dorea*. Although some of these observations were retained in PCB-exposed males versus females, other distinctive changes at the genus level include increased abundance for *Adlercruetzia* and *Dehalobacterium* in males, while PCB-exposed females showed higher abundance for *Solibacillus* and *Bifidobacterium*. Interestingly, PCB-exposed males also showed increased *Ruminococcus*, as well as *Adlercruetzia* and *Dehalobacterium* when compared to their sex-matched controls while PCB-exposed females showed increased abundance for *Solibacillus* and *Sporosarcina* in comparison to their sex-matched controls. Overall, LEfSe results showed distinguished bacterial enrichment profiles not only due to basal sex differences but also due to PCB exposure and warrant further investigations into the pathogenic and beneficial role of these enriched bacteria.

Sex-specific PCB-mediated alterations on ileal gene expression

To further explore and identify potential sex-specific PCB effects on gut properties, and how these effects could impact gut microbiome and vice versa, mRNA levels for genes encoding proteins involved in gut permeability and function were measured. Being an immunologically responsive component of the gut, in addition to its function in gut barrier maintenance, the ileum was chosen as a representative tissue for evaluation. Initial

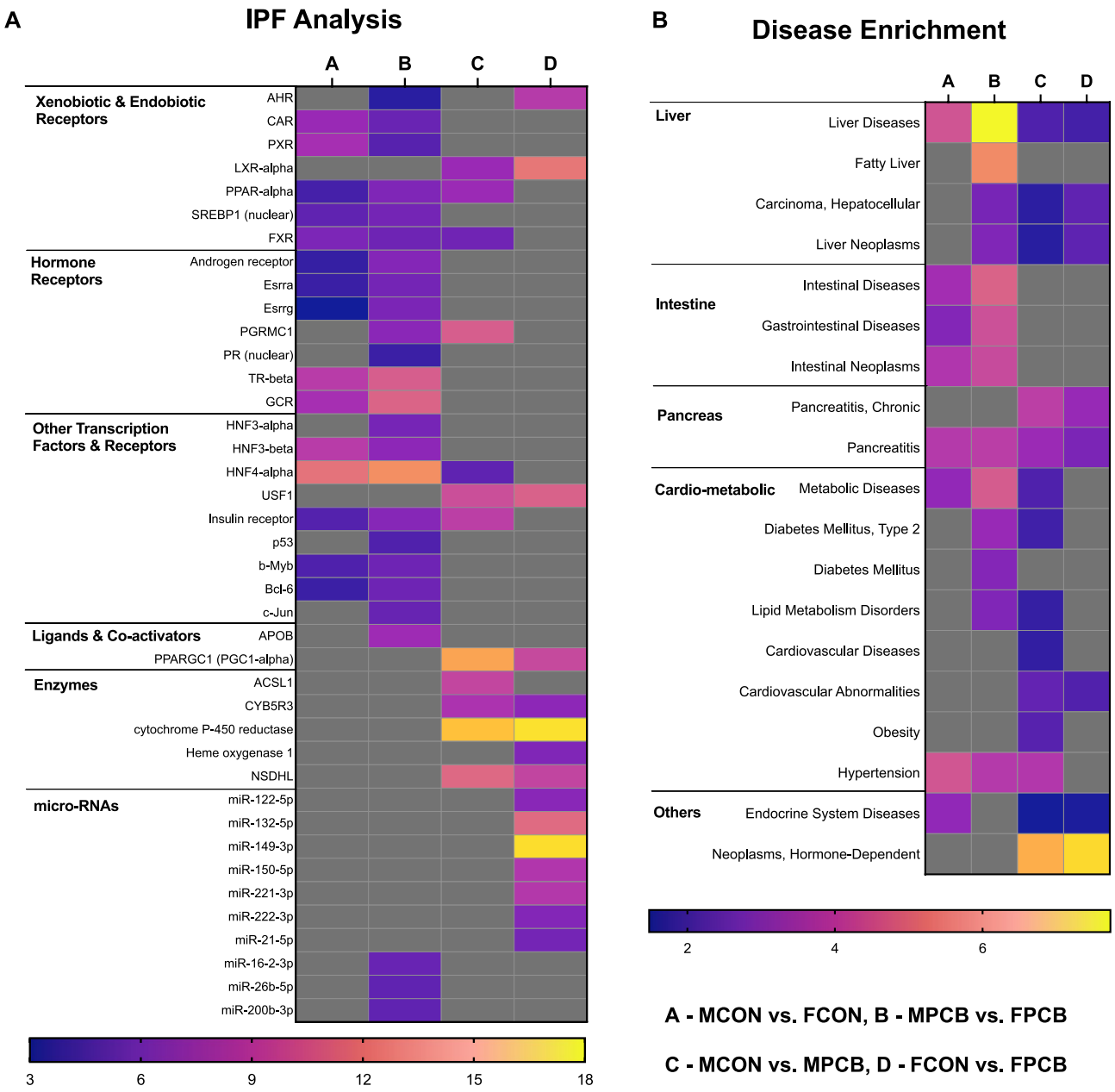

Fig. 4. Interaction by Protein Function (IPF) and Disease Enrichment analyses. (**A**) An IPF analysis was performed on the DE proteins obtained for each comparison group using MetaCore. A heat map of selected objects obtained from the IPF analysis, along with their corresponding *z*-scores, was constructed. Increased *z*-score denotes increased activity. (**B**) A disease enrichment analysis was also performed on the DE proteins for each comparison group using MetaCore and a heatmap of selected enriched diseases based on the -log(*p*-value) was constructed. A - MCON vs. FCON, B - MPCB vs. FPCB, C - MCON vs. MPCB, D - FCON vs. FPCB.

assessment of genes encoding gut barrier proteins including tight junction protein 1 (*Tjp1*), claudins (*Cldn1,2*) and occludin (*Ocln*) were carried out. While no significant sub-group differences were observed in *Tjp1*, *Cldn1* and *Cldn2* mRNA levels (Supplemental Fig. S7), significant PCB effects were noted for some genes. PCB-exposed males showed lower mRNA levels for *Ocln* (Fig. 7A) compared to their sex-matched controls. Likewise, PCB-exposed males also showed decreased expression for *Reg3g*, the gene encoding regenerating islet-derived protein 3 gamma, an anti-microbial peptide (Fig. 7B). Only a sex effect was observed for the mucin-encoding gene, *Muc1* (Fig. 7C) while no differences were observed for *Muc2* (Supplemental Fig. S7). Additionally, gene expression of healthy and functional mucosal markers, namely the cathelicidin antimicrobial peptide (*Camp*), trefoil factor 3 (*Tff3*) and fibroblast growth factor 15 (*Fgf15*) were assessed. While no sex or PCB effects were observed for *Camp*, a sex effect was observed for *Tff3* (Supplemental Fig. S7). Further, unexposed females also exhibited higher *Fgf15* mRNA levels vs. unexposed males (Fig. 7D). Finally, to evaluate xenobiotic receptor expression

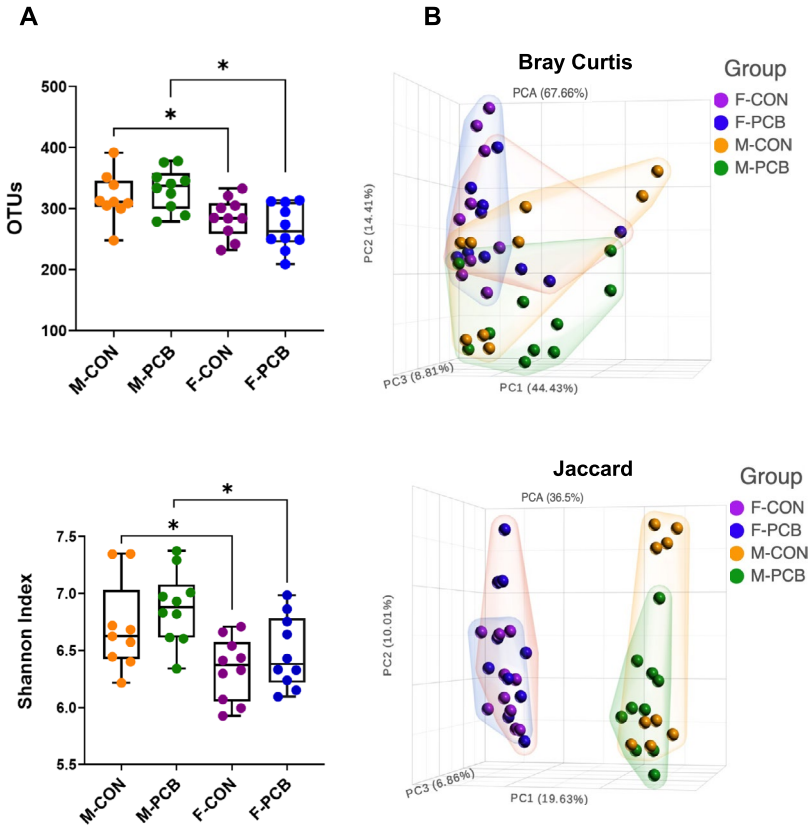

Permanova-pairwise for Bray Curtis				
Group 1	Group 2	pseudo-F	*p* -value	*q* -value
F-CON	F-PCB	1.86	0.035	0.035
F-CON	M-CON	5.31	0.001	0.002
F-CON	M-PCB	6.24	0.001	0.002
F-PCB	M-CON	3.41	0.001	0.002
F-PCB	M-PCB	3.92	0.001	0.002
M-CON	M-PCB	2.08	0.016	0.019

Permanova-pairwise for Jaccard				
Group 1	Group 2	pseudo-F	*p* -value	*q* -value
F-CON	F-PCB	1.55	0.006	0.007
F-CON	M-CON	3.75	0.001	0.002
F-CON	M-PCB	3.58	0.001	0.002
F-PCB	M-CON	3.32	0.001	0.002
F-PCB	M-PCB	3.44	0.001	0.002
M-CON	M-PCB	1.57	0.024	0.024

Fig. 5. Gut microbial composition analysis. (**A**) Alpha diversity indices namely observed species (OTUs - observed taxonomic units) and Shannon Index were calculated to measure differences in microbial diversity within individual samples. Values are mean ± SD, *Adjusted p <0.05. (**B**) Differences in microbial diversity between samples were accessed using beta diversity measures including Bray Curtis and Jaccard algorithms. PCA plots for these algorithms along with the respective Permanova-pairwise comparisons are presented.

in the gut, ileal mRNA levels of *Cyp1a1*, an AHR target gene and PCB target was measured. As expected, PCB exposure resulted in *Cyp1a1* gene induction, indicative of AHR activation (Fig. 7E). Surprisingly, sex differences were observed in ileal *Cyp1a1* induction levels with PCB-exposed males demonstrating more robust induction than exposed females despite no differences in ileal gene expression levels for the AHR (Fig. 7F).

Discussion

Emerging toxicological studies have documented sex differences in liver and metabolic phenotype with PCB exposures[15]. Epidemiological studies on historic cohorts such as the "Yucheng" population with accidental, high-dose exposures to PCBs, demonstrated that the female sex may be more susceptible to metabolic disease outcomes including diabetes[42]. Prenatal PCB exposures were also associated with significantly more obesogenic effects in female adolescents vs. males[43]. In contrast, exposure studies to dioxin-like PCBs using rodent models demonstrated that male rats and mice manifested greater susceptibility to disruption in glucose homeostasis while female rats were more predisposed to PCB126-mediated disruption in fatty acid metabolism and lipid homeostasis[15,44]. Overall, sex-specific outcomes with PCB exposures, while highly dependent on the dose, duration, and nature of exposure, reiterate the ability of these chemicals to interfere with normal metabolic and endocrine processes and interact with hepatic xenobiotic receptors as part of their mechanistic contributions to metabolic and liver toxicity.

Phenotypic observations previously reported from this study, which represent effects of both dioxin-like and non-dioxin-like PCBs, included enhanced steatosis, glucose intolerance, and inflammation in the female sex compared to their exposed male counterparts[16] (Supplemental Fig. S8). While exhibiting decreased hepatic HNF4 alpha expression, exposed female mice also showed decreased hepatic mRNA and protein levels for phosphorylated epidermal growth factor receptor (EGFR) which was interpreted as one of the plausible mechanisms for the sex-specific hepatic and metabolic toxicity[16]. It has been hypothesized that inhibition of EGFR phosphorylation by PCBs can induce hepatic signaling disruption leading to alterations in normal energy metabolism[22]. Another attributable factor for the observed sex-specific effects was the pro-androgenic and anti-estrogenic effects of this particular PCB mixture in females that fueled their sensitivity to metabolic disruption[16] given that estrogens and hepatic estrogen receptor (ER) alpha expression play critical roles in maintenance of insulin sensitivity[45], lipid homeostasis[46] and oxidative stress responses[47]. While these phenotyping findings shed

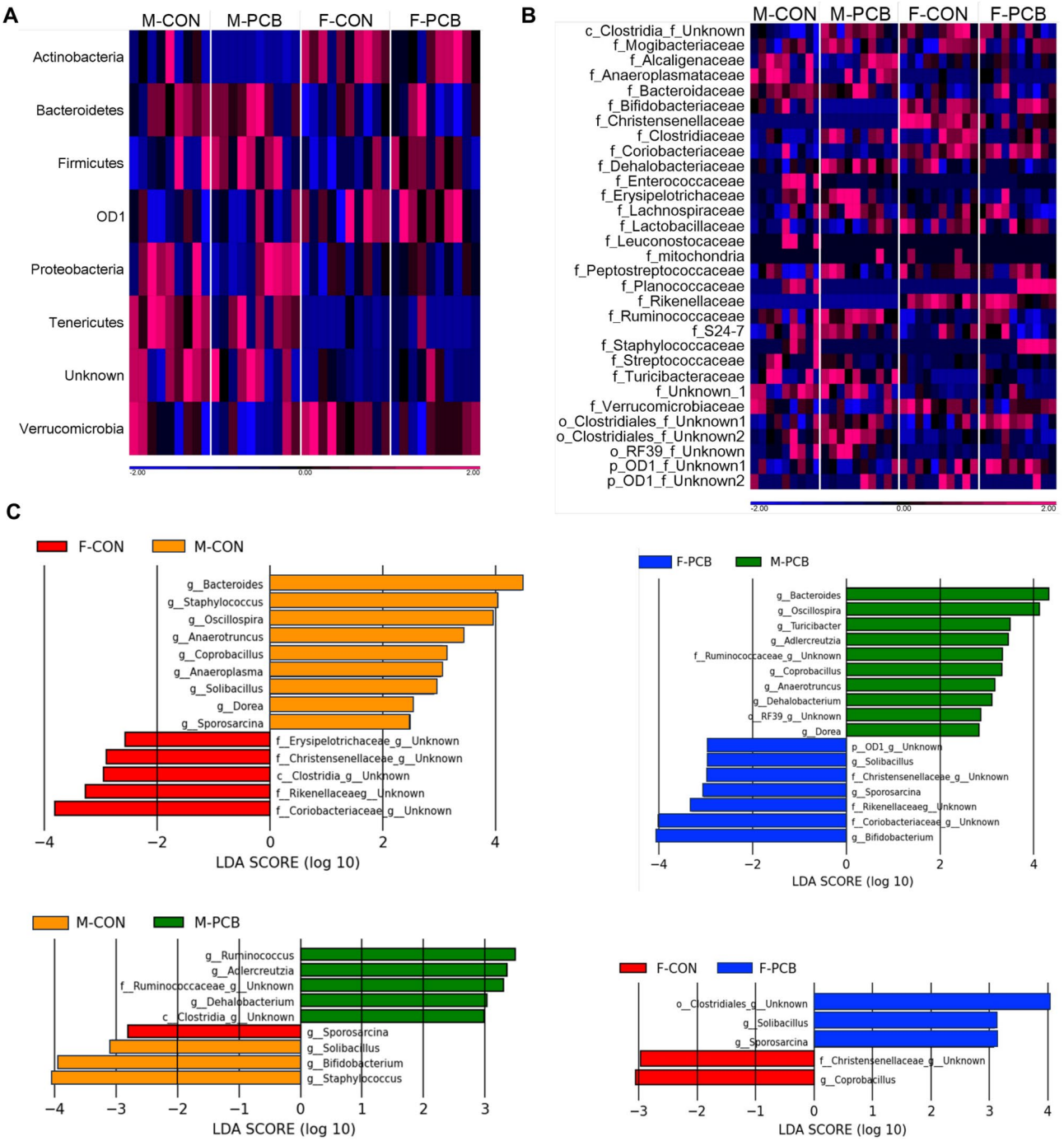

Fig. 6. Effects of sex and PCB exposure at different taxonomic levels. Heatmaps depicting bacterial abundance at the (**A**) phyla and (**B**) family levels were generated. (**C**) Linear discriminant analysis (LefSe) was performed for relative bacterial abundance at the genus level and the results for each comparison group is presented.

light on the sex-specific toxicity profile elicited by this combination of PCBs, they also suggest other off-hepatic PCB effects including potential multi-organ interactions that could have ramifications on toxicant-associated steatotic liver disease (TASLD) development.

Findings from the current study which focused on how short-term exposures to the non-dioxin-like Aroclor 1260 plus dioxin-like PCB126 affect the hepatic protein landscape in male and female mice revealed that the massive differences in protein expression were largely driven by biological sex. Higher basal protein levels for FMOs including FMO3 and multiple P450 enzymes were observed in these young adult C57BL/6 female mice compared to their male counterparts. While higher basal mRNA levels for most P450 enzymes including *Cyp2b10* and *Cyp3a11* have been reported in this mouse strain[48], the current data affirm those findings at the protein levels as well. Similarly, sex differences in hepatic expression of FMOs have also been reported[49,50], and the current

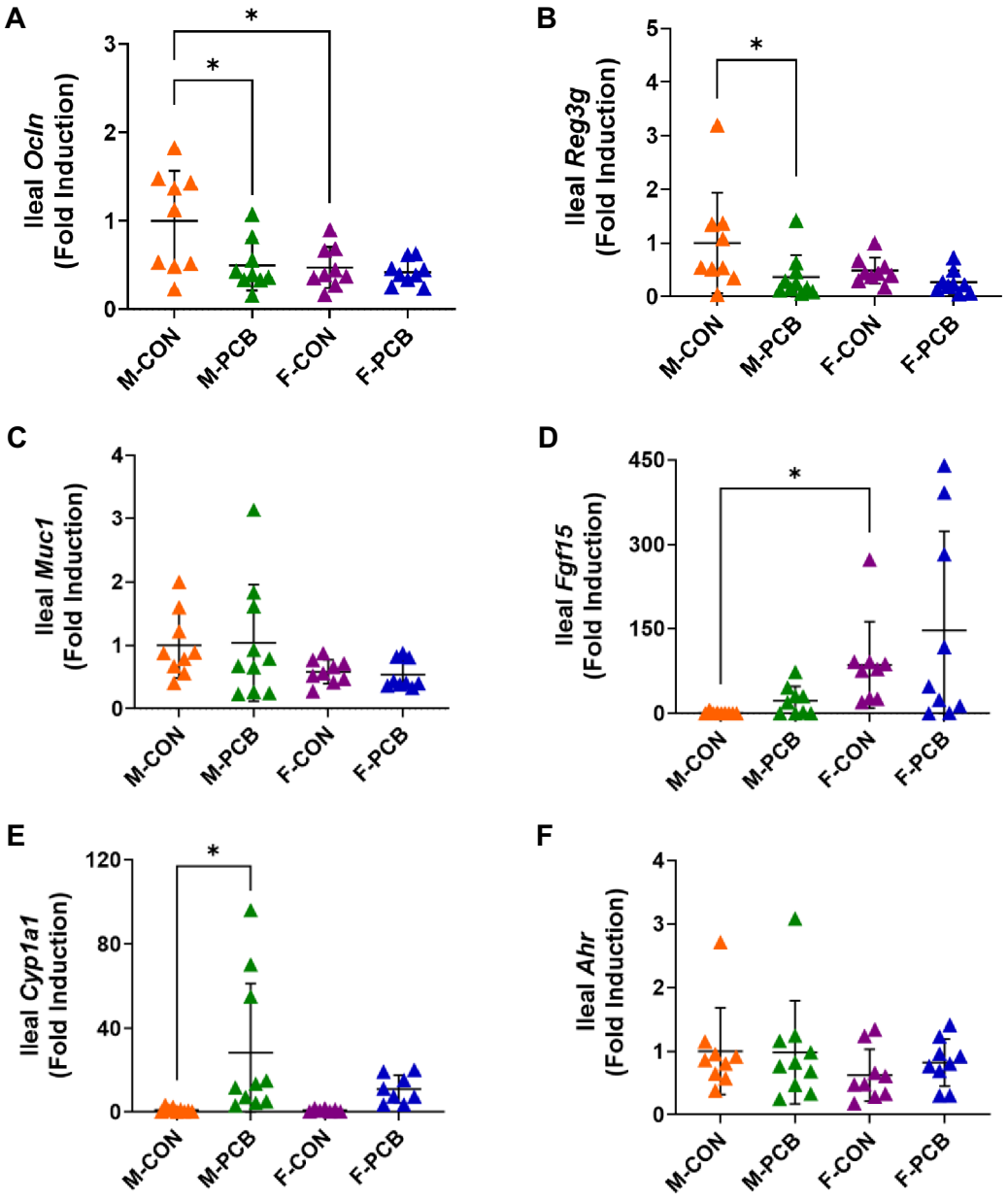

Summary of *p*-values

Endpoint	*Sex*	*PCB*	*Interaction*	*Endpoint*	*Sex*	*PCB*	*Interaction*
Ocln	**0.0129**	**0.0208**	0.0596	*Reg3g*	0.0911	**0.0211**	0.2458
Muc1	**0.0184**	0.9765	0.8224	*Fgf15*	**0.0030**	0.2139	0.5491
Cyp1a1	0.1866	**0.0070**	0.1925	*Ahr*	0.1862	0.6560	0.5855

Fig. 7. Sex and PCB effects on ileal gene expression. Ileal mRNA levels were measured for genes encoding permeability, gut mucosal, and other markers, namely (**A**) Occludin (*Ocln*), (**B**) regenerating islet-derived protein 3 gamma (*Reg3g*), (**C**) mucin 1 (*Muc1*), (**D**) fibroblast growth factor 15 (*Fgf15*), (**E**) cytochrome P450 1A1 (*Cyp1a1*) and (**F**) the aryl hydrocarbon receptor (*Ahr*). A list of *p*-values from the two-way ANOVA analysis is also provided. Values are mean ± SD, **p* <0.05.

observations are in concordance with those reports. In terms of sex-specific PCB effects, distinct upregulated proteins identified in the male exposed group included xenobiotic detoxification enzymes, primarily CYP2C29, a CAR target[51], CYP4A10, a PPAR alpha target[52], and CYP2A5, a downstream target of NRF2 activation and the AHR[53]. Strikingly, CYP2A5 (CYP2A6 in humans) is also upregulated with alcohol consumption and recognized as a mediator in alcohol-associated liver disease[54]. Additionally, other proteins involved in processes other than

xenobiotic detoxication were CYB5A, postulated to be involved in sterol biosynthesis[55], and RBP4, a vitamin A carrier in hepatocytes. Increased circulating RBP4 levels have been associated with MASLD, but reports remain controversial[56]. In contrast, HTATIP2, an oxidoreductase, was the only upregulated protein in PCB-exposed females. While numerous cancer studies have reported HTATIP2 as a tumor suppressor, hepatic HTATIP2 has been implicated in lipid metabolism, particularly lipid droplet formation[57,58]. These novel findings shed light on alternative key proteins that may be impacted by PCBs, besides the well-studied xenobiotic receptor targets.

Although the short-term PCB exposure resulted in modest changes in hepatic protein expression, it also contributed to distinct sex-specific biological processes as a consequence of the altered hepatic proteome, albeit both sexes showing AHR signaling (CYP1A1, CYP1A2 upregulation) as an enriched pathway. Indeed, IPF analysis suggested that AHR and LXR activation were more pronounced responses in the female sex and calls to attention the likelihood of sex-specific AHR activation by exogenous ligands which may partially account for differences in toxicity outcomes, and susceptibility of female livers to changes in lipid metabolism with toxicant exposures. Furthermore, when compared to exposed males, PCB-exposed females also exhibited increased protein expression for CD36, accompanied by disease enrichment for "fatty liver" in this group. CD36 is a fatty acid translocating protein and shared AHR target gene. Upregulated CD36 expression by the classic AHR ligand, TCDD, have been partially credited for increased steatosis with high-fat dietary intake[59,60]. It should be noted however, that biological sex largely drove the differences in lipid processes as observed in the GO Process findings, while the PCB effects were modest. Further, "estradiol metabolism" was identified as the most enriched pathway in the PCB-exposed female group, possibly as a consequence of the augmented AHR activation. AHR-ER interactions have been confirmed through in vitro studies, and increased AHR activation is often associated with dampened ER signaling and reduced estrogen levels[61]. Although the current study did not record a significant decrease in estradiol (E2) circulatory levels in the PCB-exposed group, a nonsignificant trend was observed[16].

In conformity with the proteomic results, metagenomic analyses also exemplified how biological sex majorly drives changes in microbial diversity. Our findings demonstrated that Actinobacteria and Tenericutes were more abundant in male mice while female mice have lower Bacteroidetes abundance. While these findings reaffirmed previous reports on sex differences in gut microbiota in experimental models[62,63], they also supported evidence of sex differences in human gut microbiome studies wherein female participants displayed lower Bacteroidetes abundance[64]. PCB exposure also impacted microbial composition differently in males and females. One intriguing observation was the sex-specific impact of PCB exposure on bacterial abundance noted by the greater abundance of *Bifidobacteriaceae*, a key bacterial family involved in bile acid metabolism, in PCB-exposed females but not males. Basal sex differences in secondary bile acid levels have been reported with females exhibiting higher secondary bile acids than males[65], and this may subsequently affect the abundance of bile acid metabolizing bacteria. Although bile acids are yet to be measured in the current study, our findings suggest that PCB exposure may potentially modify bile acid composition through gut microbiota changes specifically in females. Importantly, bile acid-mediated effects on gut microbiota have been postulated as a pathway in regulation of lipid metabolism genes and overall metabolic homeostasis[65]. Increased levels of *Bifidobacterium*, a bacterial genus strongly correlated with carbohydrate metabolism, butyrate production and host health benefits[66], was also observed in PCB-exposed females but not males and appear contradictory when considering the observed phenotypic findings in the female sex. Even though basal sex differences may act as a driver for the increased *Bifidobacterium* in PCB-exposed females, PCB-mediated effects in carbohydrate metabolism observed in this group may also act as a probable driver stimulating growth and possibly metabolic activity of this particular genus[67]. Nonetheless, the current study only accounted for acute effects with exposure and longer-term exposures may not necessarily reflect these patterns. Another compelling sex-specific observation in the current study was the increased abundance of *Dehalobacterium* only in PCB-exposed males. This is fascinating given that the *Dehalobacter* genus constitutes of bacterial populations implicated exclusively in degradation of organohalides such as dichloromethane[68,69]. As organohalides, PCBs, especially higher molecular weight congeners, are also subjected to microbial degradation through de-chlorination under anaerobic conditions. In fact, utilization of PCB dechlorinating bacteria including *Dehalococcoides* sp. has been successfully embraced as a strategy in PCB remediation efforts on contaminated soil and water[70]. Thus, it can be postulated that the increased abundance in *Dehalobacterium* with PCB exposure may, in part, serve as a bacterial response to the presence of parent organohalides and/or their metabolites in the gut. One plausible explanation for the observed *Dehalobacterium* abundance only in males could be differences in PCB gut distribution and bioaccumulation between males and females. This is also supported by the observed sex-specific induction of ileal *Cyp1a1* in males but not females, although this observation also suggests that AHR activation by PCBs may be tissue-specific contingent on sex. However, a better understanding as to why this microbial compositional change is observed only in males with PCB exposure remains to be elucidated.

The hepatic proteome-gut microbiome data, coupled with our previously reported phenotyping observations, offered a more nuanced outlook on PCBs' contribution to metabolic dysfunction and TASLD/TASH outcomes. The findings suggest that, in addition to biological sex, organ-organ interactions should be considered when predicting toxicity outcomes with environmental exposures especially for persistent compounds such as PCBs that can impact multiple organs simultaneously yet have tissue-specific effects. Particularly, these toxicity effects may not be concerted and appear somewhat dissociative. Regardless, the current findings underscore major sex-specific mechanistic pathways implicated in these toxicity phenotypes including sensitivity of female mice to hepatic AHR activation and repercussions thereof on hepatic estrogen metabolism and overall energy homeostasis.

Despite the current study's strength in identifying mechanistic pathways with toxicant exposures using omics platforms, it is not without limitations. Firstly, the use of a short-term study design may not necessarily capture human exposure paradigms which are often chronic and occur over time. The minimal protein alterations

observed with PCBs could also be due to the short period of exposure, with some computational analyses driven by a modest number of DE proteins, specifically the FCON vs. FPCB group. Secondly, the study did not reckon in its analyses, how phases of the estrus cycle in female mice may have influenced the measured endpoints for this sex. Further, while investigating gut microbiota changes, the study did not extend towards functional analyses and bacterial metabolite profile. Significantly, the study only considered environmental factors albeit TASLD often requiring more than one "hit" to develop and progress[4]. The unequal sample sizes for the proteomics vs.16S RNA sequencing experiments also limited the ability to perform integrated bioinformatic analyses specific to each mouse. Lastly, PCB body burdens were not assessed in the current study. In reconciliation with these current study limitations, future studies will include performing longer-term exposures in the presence of additional factors such as hypercaloric diets and other relevant lifestyle factors to better translate our research findings to exposed and affected populations. Use of whole genome sequencing and expanding the analysis on gut microbiota profile to functional metagenomics will also provide an in-depth picture on PCB effects on the gut and consequent impact of those changes on metabolic homeostasis. Further, future multi-omic platforms will also incorporate uniform sample sizes for integrated multi-omic analyses.

Conclusions

In closing, the present study provided valuable information on sex differences in the hepatic proteome and gut microbiome in the routinely used C57BL/6 mouse strain. Importantly, the current findings highlighted how acute PCB exposures transform the liver protein landscape in female mice, which is currently unknown knowledge, and provided insights on prospective mechanisms steering the sex-specific TASLD endpoints observed. In particular, only modest observations were made with regards to sex-specific DE proteins with PCB exposures. Nonetheless, the current study presented a perspective on how off-liver PCB effects may also promote sex-specific TASLD/metabolic outcomes. Furthermore, the omics data also aid in hypothesis generation and fueling additional research questions such as the consequential impact of liver vs. intestinal AHR activation with PCB exposures and underlying sex differences; impact of PCBs on bile acid metabolism; sex differences in PCB distribution and bioaccumulation and how that consequentially modulates gut-liver toxicity; and lastly, how long-term PCB exposure can affect intestinal permeability and function.

Data availability

Raw proteomic data files were deposited in MassIVE (http://massive.ucsd.edu/) data repository (MassIVE ID: MSV000096056) maintained by the Center for Computational Mass Spectrometry at the University of California, San Diego. These data included i) primary data files (.RAW) for the 2DLC-MS fractionated liver TMT-labeled tryptic lysates, ii) an excel file with assembled Proteome Discoverer v2.5 search results, iii) the sample key, and (iv) the mouse reviewed canonical (download: March 17, 2023) FASTA sequence database. Raw sequencing data files have been uploaded to the Sequence Read Archive database (BioProject ID: PRJNA1168501) with the following reviewer link https://dataview.ncbi.nlm.nih.gov/object/PRJNA1168501?reviewer=7kmcoj5a4nutpd3gr2scdclhqd. All data will be made publicly available upon manuscript acceptance. Data access can also be obtained upon request from the corresponding author.

Received: 6 June 2025; Accepted: 8 October 2025
Published online: 14 November 2025

References

1. Markowitz, G. & Rosner, D. Monsanto, PCBs, and the creation of a "world-wide ecological problem". *J Pub. Health Polic.* **39**, 463–540. https://doi.org/10.1057/s41271-018-0146-8 (2018).
2. Wang, Z. et al. Inflammation and cardiometabolic diseases induced by persistent organic pollutants and nutritional interventions: Effects of multi-organ interactions. *Environ. Pollut.* **339**, 122756. https://doi.org/10.1016/j.envpol.2023.122756 (2023).
3. Peng, F. J. et al. Association of hair polychlorinated biphenyls and multiclass pesticides with obesity, diabetes, hypertension and dyslipidemia in NESCAV study. *J. Hazard Mat.* **461**, 132637. https://doi.org/10.1016/j.jhazmat.2023.132637 (2024).
4. Wahlang, B. et al. Mechanisms of environmental contributions to fatty liver disease. *Curr. Environ. Health Rep.* **6**, 80–94. https://doi.org/10.1007/s40572-019-00232-w (2019).
5. Wu, B. et al. Combined exposure to multiple dioxins and dioxin-like polychlorinated biphenyls on hypertension among US adults in NHANES: A cross-sectional study under three statistical models. *Environ. Sci. Pollut. Res. Int.* **30**, 28730–28744. https://doi.org/10.1007/s11356-022-24271-3 (2023).
6. Pavuk, M. et al. Polychlorinated biphenyls, polychlorinated dibenzo-p-dioxins, polychlorinated dibenzofurans, pesticides, and diabetes in the Anniston community health survey follow-up (ACHS II): single exposure and mixture analysis approaches. *Sci. Total Environ.* **877**, 162920. https://doi.org/10.1016/j.scitotenv.2023.162920 (2023).
7. Wahlang, B., Hardesty, J. E., Jin, J., Falkner, K. C. & Cave, M. C. Polychlorinated biphenyls and nonalcoholic fatty liver disease. *Curr. Opin. Toxicol.* **14**, 21–28. https://doi.org/10.1016/j.cotox.2019.06.001 (2019).
8. Cousins, I. T., Ng, C. A., Wang, Z. & Scheringer, M. Why is high persistence alone a major cause of concern?. *Environ. Sci. Proc. Impact.* **21**, 781–792. https://doi.org/10.1039/c8em00515j (2019).
9. National report on human exposure to environmental chemicals. Biomonitoring data tables for environmental chemicals. *centers for disease control and prevention (CDC). U.S. Department of Health and Human Services, Public Health Service* https://www.cdc.gov/exposurereport/index.html.
10. Safe, S. Toxicology, structure-function relationship, and human and environmental health impacts of polychlorinated biphenyls: Progress and problems. *Environ. Health Perspect.* **100**, 259–268. https://doi.org/10.1289/ehp.93100259 (1993).
11. Wahlang, B. et al. Human receptor activation by aroclor 1260, a polychlorinated biphenyl mixture. *Toxicol. Sci.* **140**, 283–297. https://doi.org/10.1093/toxsci/kfu083 (2014).
12. Wahlang, B. et al. Evaluation of Aroclor 1260 exposure in a mouse model of diet-induced obesity and non-alcoholic fatty liver disease. *Toxicol. Appl. Pharmacol.* **279**, 380–390. https://doi.org/10.1016/j.taap.2014.06.019 (2014).
13. Head, K. Z. et al. Investigating the effects of long-term Aroclor 1260 exposure on fatty liver disease in a diet-induced obesity mouse model. *Front. Gastroenterol. (Lausanne)* https://doi.org/10.3389/fgstr.2023.1180712 (2023).

14. Wahlang, B. et al. Editor's highlight: PCB126 exposure increases risk for peripheral vascular diseases in a liver injury mouse model. *Toxicol. Sci.* **160**, 256–267. https://doi.org/10.1093/toxsci/kfx180 (2017).
15. Wahlang, B. Rising STARS: Sex differences in toxicant-associated fatty liver disease. *J. Endocrinol.* https://doi.org/10.1530/JOE-22-0247 (2023).
16. Wahlang, B. et al. Identifying sex differences arising from polychlorinated biphenyl exposures in toxicant-associated liver disease. *Food Chem. Toxicol.* **129**, 64–76. https://doi.org/10.1016/j.fct.2019.04.007 (2019).
17. Younossi, Z. M. et al. The global epidemiology of non-alcoholic fatty liver disease and non-alcoholic steatohepatitis among patients with type 2 diabetes. *Clin. Gastroenterol. Hepatol.* https://doi.org/10.1016/j.cgh.2024.03.006 (2024).
18. Wahlang, B. et al. polychlorinated biphenyl-xenobiotic nuclear receptor interactions regulate energy metabolism, behavior, and inflammation in non-alcoholic-steatohepatitis. *Toxicol. Sci.* **149**, 396–410. https://doi.org/10.1093/toxsci/kfv250 (2016).
19. Gadupudi, G. S. et al. PCB126 inhibits the activation of AMPK-CREB signal transduction required for energy sensing in liver. *Toxicol. Sci.* **163**, 440–453. https://doi.org/10.1093/toxsci/kfy041 (2018).
20. Wahlang, B. Exposure to persistent organic pollutants: Impact on women's health. *Rev. Environ. Health* **33**, 331–348. https://doi.org/10.1515/reveh-2018-0018 (2018).
21. Ruan, J. et al. Adolescent exposure to environmental level of PCBs (Aroclor 1254) induces non-alcoholic fatty liver disease in male mice. *Environ. Res.* **181**, 108909. https://doi.org/10.1016/j.envres.2019.108909 (2020).
22. Hardesty, J. E. et al. Polychlorinated biphenyls disrupt hepatic epidermal growth factor receptor signaling. *Xenobiotica* **47**, 807–820. https://doi.org/10.1080/00498254.2016.1217572 (2017).
23. Hardesty, J. E. et al. Hepatic signalling disruption by pollutant Polychlorinated biphenyls in steatohepatitis. *Cell Signal* **53**, 132–139. https://doi.org/10.1016/j.cellsig.2018.10.004 (2019).
24. Petri, B. J. et al. Polychlorinated biphenyls alter hepatic m6A mRNA methylation in a mouse model of environmental liver disease. *Environ. Res.* **216**, 114686. https://doi.org/10.1016/j.envres.2022.114686 (2023).
25. Piell, K. M. et al. Disruption of the mouse liver epitranscriptome by long-term aroclor 1260 exposure. *Environ. Toxicol. Pharmacol.* **100**, 104138. https://doi.org/10.1016/j.etap.2023.104138 (2023).
26. Wahlang, B. et al. Polychlorinated biphenyls altered gut microbiome in CAR and PXR knockout mice exhibiting toxicant-associated steatohepatitis. *Toxicol. Rep.* **8**, 536–547. https://doi.org/10.1016/j.toxrep.2021.03.010 (2021).
27. Li, X., Liu, Y., Martin, J. W., Cui, J. Y. & Lehmler, H. J. Nontarget analysis reveals gut microbiome-dependent differences in the fecal PCB metabolite profiles of germ-free and conventional mice. *Environ. Pollut.* **268**, 115726. https://doi.org/10.1016/j.envpol.2020.115726 (2021).
28. Goncharov, A., Pavuk, M. & Foushee, H. R. Carpenter, D. O.Anniston environmental health reseach, C. Blood pressure in relation to concentrations of PCB congeners and chlorinated pesticides. *Environ. Health Perspect.* **119**, 319–325. https://doi.org/10.1289/ehp.1002830 (2011).
29. Cave, M. et al. Polychlorinated biphenyls, lead, and mercury are associated with liver disease in American adults: NHANES 2003–2004. *Environ. Health Perspect.* **118**, 1735–1742. https://doi.org/10.1289/ehp.1002720 (2010).
30. National Toxicology, P. Toxicology and carcinogenesis studies of a binary mixture of 3,3',4,4',5-pentachlorobiphenyl (PCB 126) (Cas No. 57465-28-8) and 2,2',4,4',5,5'-hexachlorobiphenyl (PCB 153) (CAS No. 35065-27-1) in female Harlan Sprague-Dawley rats (gavage studies). *Natl Toxicol Program Tech Rep Ser*, 1-258 (2006).
31. Bolstad, B. M., Irizarry, R. A., Astrand, M. & Speed, T. P. A comparison of normalization methods for high density oligonucleotide array data based on variance and bias. *Bioinformatics* **19**, 185–193. https://doi.org/10.1093/bioinformatics/19.2.185 (2003).
32. Ritchie, M. E. et al. limma powers differential expression analyses for RNA-sequencing and microarray studies. *Nucl. Acid. Res.* **43**, e47. https://doi.org/10.1093/nar/gkv007 (2015).
33. Benjamini, Y. & Hochberg, Y. Controlling the false discovery rate: A practical and powerful approach to multiple testing. *J. Roy. Stat. Soc.: Ser. B (Methodol.)* **57**, 289–300 (1995).
34. Hall, M. & Beiko, R. G. 16S rRNA gene analysis with QIIME2. *Method. Mol Biol* **113–129**, 2018. https://doi.org/10.1007/978-1-4939-8728-3_8 (1849).
35. Andrews, S. FastQC: A quality control tool for high throughput sequence data. Available:http://www.bioinformatics.babraham.ac.uk/projects/fastqc/. (2015).
36. Callahan, B. J. et al. DADA2: High-resolution sample inference from Illumina amplicon data. *Nat. Method.* **13**, 581–583. https://doi.org/10.1038/nmeth.3869 (2016).
37. DeSantis, T. Z. et al. Greengenes, a chimera-checked 16S rRNA gene database and workbench compatible with ARB. *Appl. Environ. Microbiol.* **72**, 5069–5072. https://doi.org/10.1128/AEM.03006-05 (2006).
38. Storey, J. D. The positive false discovery rate: A Bayesian interpretation and the q-value. *Ann. Stat.* **31**, 2013–2035 (2003).
39. Segata, N. et al. Metagenomic biomarker discovery and explanation. *Genom. Biol.* **12**, R60. https://doi.org/10.1186/gb-2011-12-6-r60 (2011).
40. Xie, F., Wang, J. & Zhang, B. RefFinder: A web-based tool for comprehensively analyzing and identifying reference genes. *Funct. Integr. Genom.* **23**, 125. https://doi.org/10.1007/s10142-023-01055-7 (2023).
41. Rada, P., Gonzalez-Rodriguez, A., Garcia-Monzon, C. & Valverde, A. M. Understanding lipotoxicity in NAFLD pathogenesis: Is CD36 a key driver?. *Cell Death Dis.* **11**, 802. https://doi.org/10.1038/s41419-020-03003-w (2020).
42. Wang, S. L., Tsai, P. C., Yang, C. Y. & Guo, Y. L. Increased risk of diabetes and polychlorinated biphenyls and dioxins: a 24-year follow-up study of the Yucheng cohort. *Diabet. Care* **31**, 1574–1579. https://doi.org/10.2337/dc07-2449 (2008).
43. Tang-Peronard, J. L. et al. Association between prenatal polychlorinated biphenyl exposure and obesity development at ages 5 and 7 y: A prospective cohort study of 656 children from the Faroe Islands. *Am. J. Clin. Nutr.* **99**, 5–13. https://doi.org/10.3945/ajcn.113.066720 (2014).
44. Eti, N. A. et al. PCB126 induced toxic actions on liver energy metabolism is mediated by AhR in rats. *Toxicology* **466**, 153054. https://doi.org/10.1016/j.tox.2021.153054 (2022).
45. De Paoli, M., Zakharia, A. & Werstuck, G. H. The role of estrogen in insulin resistance: A review of clinical and preclinical data. *Am. J. Pathol.* **191**, 1490–1498. https://doi.org/10.1016/j.ajpath.2021.05.011 (2021).
46. Goossens, G. H., Jocken, J. W. E. & Blaak, E. E. Sexual dimorphism in cardiometabolic health: The role of adipose tissue, muscle and liver. *Nat. Rev. Endocrinol.* **17**, 47–66. https://doi.org/10.1038/s41574-020-00431-8 (2021).
47. Iorga, A. et al. The protective role of estrogen and estrogen receptors in cardiovascular disease and the controversial use of estrogen therapy. *Biol. Sex Differ.* **8**, 33. https://doi.org/10.1186/s13293-017-0152-8 (2017).
48. Luo, J., Watson, W. H., Gripshover, T. C., Qaissi, Z. & Wahlang, B. Sex-specific effects of acute chlordane exposure in the context of steatotic liver disease, energy metabolism and endocrine disruption. *Food Chem. Toxicol.* **180**, 114024. https://doi.org/10.1016/j.fct.2023.114024 (2023).
49. Celius, T. et al. Aryl hydrocarbon receptor-dependent induction of flavin-containing monooxygenase mRNAs in mouse liver. *Drug Metab. Dispos.* **36**, 2499–2505. https://doi.org/10.1124/dmd.108.023457 (2008).
50. Janmohamed, A., Hernandez, D., Phillips, I. R. & Shephard, E. A. Cell-, tissue-, sex- and developmental stage-specific expression of mouse flavin-containing monooxygenases (Fmos). *Biochem. Pharmacol.* **68**, 73–83. https://doi.org/10.1016/j.bcp.2004.02.036 (2004).
51. Hernandez, J. P., Mota, L. C., Huang, W., Moore, D. D. & Baldwin, W. S. Sexually dimorphic regulation and induction of P450s by the constitutive androstane receptor (CAR). *Toxicology* **256**, 53–64. https://doi.org/10.1016/j.tox.2008.11.002 (2009).

52. Su, S. et al. The role of mouse and human peroxisome proliferator-activated receptor-alpha in modulating the hepatic effects of perfluorooctane sulfonate in mice. *Toxicology* **465**, 153056. https://doi.org/10.1016/j.tox.2021.153056 (2022).
53. Abu-Bakar, A. et al. Function and regulation of the Cyp2a5/CYP2A6 genes in response to toxic insults in the liver. *Curr. Drug Metab.* **14**, 137–150 (2013).
54. Leung, T. M. & Lu, Y. Alcoholic liver disease: From CYP2E1 to CYP2A5. *Curr. Mol. Pharmacol.* **10**, 172–178. https://doi.org/10.2174/1874467208666150817111846 (2017).
55. Ma, M. Y. et al. Defects in CYB5A and CYB5B impact sterol-C4 oxidation in cholesterol biosynthesis and demonstrate regulatory roles of dimethyl sterols. *Cell Rep.* **43**, 114912. https://doi.org/10.1016/j.celrep.2024.114912 (2024).
56. Hu, R., Yang, X., He, X. & Song, G. The relationship between NAFLD and retinol-binding protein 4 - an updated systematic review and meta-analysis. *Lipid. Health Dis.* **22**, 8. https://doi.org/10.1186/s12944-022-01771-2 (2023).
57. Liao, B. M. et al. Proteomic analysis of livers from fat-fed mice deficient in either PKCdelta or PKCepsilon identifies Htatip2 as a regulator of lipid metabolism. *Proteomics* **14**, 2578–2587. https://doi.org/10.1002/pmic.201400202 (2014).
58. Huang, L. et al. Subcongenic analysis of a quantitative trait locus affecting body weight and glucose metabolism in zinc transporter 7 (znt7)-knockout mice. *BMC Genet* **20**, 19. https://doi.org/10.1186/s12863-019-0715-2 (2019).
59. Angrish, M. M., Mets, B. D., Jones, A. D. & Zacharewski, T. R. Dietary fat is a lipid source in 2,3,7,8-tetrachlorodibenzo-rho-dioxin (TCDD)-elicited hepatic steatosis in C57BL/6 mice. *Toxicol. Sci.* **128**, 377–386. https://doi.org/10.1093/toxsci/kfs155 (2012).
60. Cong, Y. et al. 2,3,7,8-Tetrachlorodibenzo-p-dioxin induces liver lipid metabolism disorder via the ROS/AMPK/CD36 signaling pathway. *Toxicol. Sci.* **191**, 276–284. https://doi.org/10.1093/toxsci/kfac133 (2023).
61. Tarnow, P., Tralau, T. & Luch, A. Chemical activation of estrogen and aryl hydrocarbon receptor signaling pathways and their interaction in toxicology and metabolism. *Expert. Opin. Drug Metab. Toxicol.* **15**, 219–229. https://doi.org/10.1080/17425255.2019.1569627 (2019).
62. Org, E. et al. Sex differences and hormonal effects on gut microbiota composition in mice. *Gut Microb.* **7**, 313–322. https://doi.org/10.1080/19490976.2016.1203502 (2016).
63. Kim, Y. S., Unno, T., Kim, B. Y. & Park, M. S. Sex differences in gut microbiota. *World J. Men. Health* **38**, 48–60. https://doi.org/10.5534/wjmh.190009 (2020).
64. Dominianni, C. et al. Sex, body mass index, and dietary fiber intake influence the human gut microbiome. *PLoS ONE* **10**, e0124599. https://doi.org/10.1371/journal.pone.0124599 (2015).
65. Baars, A. et al. Sex differences in lipid metabolism are affected by presence of the gut microbiota. *Sci. Rep.* **8**, 13426. https://doi.org/10.1038/s41598-018-31695-w (2018).
66. O'Callaghan, A. & van Sinderen, D. Bifidobacteria and their role as members of the human gut microbiota. *Front. Microbiol.* **7**, 925. https://doi.org/10.3389/fmicb.2016.00925 (2016).
67. Pokusaeva, K., Fitzgerald, G. F. & van Sinderen, D. Carbohydrate metabolism in Bifidobacteria. *Genes Nutr.* **6**, 285–306. https://doi.org/10.1007/s12263-010-0206-6 (2011).
68. Adrian, L. & Löffler, F. E. *Organohalide-respiring bacteria*. **85** (Springer, 2016).
69. Puentes Jacome, L. A. & Edwards, E. A. A switch of chlorinated substrate causes emergence of a previously undetected native Dehalobacter population in an established Dehalococcoides-dominated chloroethene-dechlorinating enrichment culture. *FEMS Microbiol. Ecol.* https://doi.org/10.1093/femsec/fix141 (2017).
70. Sowers, K. R. & May, H. D. In situ treatment of PCBs by anaerobic microbial dechlorination in aquatic sediment: are we there yet?. *Curr. Opin. Biotechnol.* **24**, 482–488. https://doi.org/10.1016/j.copbio.2012.10.004 (2013).

Acknowledgements

The authors would like to acknowledge Sabine J. Waigel and Vennila Arumugam for their assistance with the 16S sequencing, and Daniel W. Wilkey for his assistance with the proteomic experiments. The authors would also like to acknowledge Shesh N. Rai and Sudhir Srivastava for their input in the proteomic analyses, and the CIEHS Core Utilization Subsidy Program (CUSP) for financial assistance with the project.

Author contributions

Richa A. Singhal: Formal analysis, Investigation, Writing - Original Draft, Writing - Review & Editing, Visualization. Zayna Qaissi: Investigation, Writing - Review & Editing. Hao Zheng: Formal analysis, Writing - Review & Editing, Visualization. Yuan Hua - Investigation. Josiah E. Hardesty: Methodology, Investigation, Writing - Review & Editing. Eric C. Rouchka: Formal analysis, Resources, Visualization, Project administration. Michael L. Merchant: Investigation, Resources, Project administration. Maiying Kong: Formal analysis, Resources, Writing - Review & Editing, Project administration. Banrida Wahlang: Conceptualization, Methodology, Formal analysis, Investigation, Resources, Writing - Original Draft, Writing - Review & Editing, Visualization, Supervision, Project administration, Funding acquisition.

Funding

This research was supported, in part, by the National Institute of Environmental Health Sciences (K01ES033289, P42ES023716, P30ES030283); the National Institute of General Medical Sciences (P20GM113226, P20GM103436), the Department of Defense Toxic Exposure Research Program (HT94252310949), and the Jewish Heritage Fund Research Recruitment Grant Program at the University of Louisville, School of Medicine.

Declaration

Competing interests

The authors declare no competing interests.

Additional information

Supplementary Information The online version contains supplementary material available at https://doi.org/10.1038/s41598-025-23603-w.

Correspondence and requests for materials should be addressed to B.W.